

University of Kentucky

UKnowledge

Theses and Dissertations--Chemical and Materials Engineering

**Chemical and Materials Engineering** 

2020

# EFFECT OF SILICA NANOCONFINEMENT OF LIPID BILAYERS ON ITS PHASE TRANSITION AND ON THE COLLOIDAL STABILITY OF SILICA NANOPARTICLES

Aniruddha Atul Shirodkar *University of Kentucky*, aa.prabhushirodkar@gmail.com

Author ORCID Identifier:

https://orcid.org/0000-0001-5077-8556

Digital Object Identifier: https://doi.org/10.13023/etd.2020.165

Right click to open a feedback form in a new tab to let us know how this document benefits you.

#### **Recommended Citation**

Shirodkar, Aniruddha Atul, "EFFECT OF SILICA NANOCONFINEMENT OF LIPID BILAYERS ON ITS PHASE TRANSITION AND ON THE COLLOIDAL STABILITY OF SILICA NANOPARTICLES" (2020). *Theses and Dissertations—Chemical and Materials Engineering*. 116. https://uknowledge.uky.edu/cme\_etds/116

This Master's Thesis is brought to you for free and open access by the Chemical and Materials Engineering at UKnowledge. It has been accepted for inclusion in Theses and Dissertations--Chemical and Materials Engineering by an authorized administrator of UKnowledge. For more information, please contact UKnowledge@lsv.uky.edu.

#### STUDENT AGREEMENT:

I represent that my thesis or dissertation and abstract are my original work. Proper attribution has been given to all outside sources. I understand that I am solely responsible for obtaining any needed copyright permissions. I have obtained needed written permission statement(s) from the owner(s) of each third-party copyrighted matter to be included in my work, allowing electronic distribution (if such use is not permitted by the fair use doctrine) which will be submitted to UKnowledge as Additional File.

I hereby grant to The University of Kentucky and its agents the irrevocable, non-exclusive, and royalty-free license to archive and make accessible my work in whole or in part in all forms of media, now or hereafter known. I agree that the document mentioned above may be made available immediately for worldwide access unless an embargo applies.

I retain all other ownership rights to the copyright of my work. I also retain the right to use in future works (such as articles or books) all or part of my work. I understand that I am free to register the copyright to my work.

#### REVIEW, APPROVAL AND ACCEPTANCE

The document mentioned above has been reviewed and accepted by the student's advisor, on behalf of the advisory committee, and by the Director of Graduate Studies (DGS), on behalf of the program; we verify that this is the final, approved version of the student's thesis including all changes required by the advisory committee. The undersigned agree to abide by the statements above.

Aniruddha Atul Shirodkar, Student

Dr. Barbara L. Knutson, Major Professor

Dr. Stephen E. Rankin, Director of Graduate Studies

### EFFECT OF SILICA NANOCONFINEMENT OF LIPID BILAYERS ON ITS PHASE TRANSITION AND ON THE COLLOIDAL STABILITY OF SILICA NANOPARTICLES

#### **THESIS**

A thesis submitted in partial fulfilment of the requirements for the degree of Master of Science in Chemical Engineering in the College of Engineering at the University of Kentucky

By

Aniruddha Atul Shirodkar

Lexington, Kentucky

Co- Directors: Dr. Barbara L. Knutson, Professor of Chemical Engineering and Dr. Stephen E. Rankin, Professor of Chemical Engineering Lexington, Kentucky

2020

Copyright © Aniruddha Atul Shirodkar 2020 https://orcid.org/0000-0001-5077-8556

#### ABSTRACT OF THESIS

### EFFECT OF SILICA NANOCONFINEMENT OF LIPID BILAYERS ON ITS PHASE TRANSITION AND ON THE COLLOIDAL STABILITY OF SILICA NANOPARTICLES

In this work, we incorporated 4-(N-Boc-aminometyl) phenylboronic acid (BA), at different concentrations, into 1,2-dipalmitoyl-sn-glycero-3- phosphocholine (DPPC) bilayers confined within nanopores of two different mean pore diameters of 7.4 nm and 11.7 nm of micron sized silica particles. The confinement of DPPC into nanopores resulted in the depression in the main phase transition temperatures compared to the liposomal system. The addition of BA was found to induce disruptions in the acyl chains of the lipid molecules at all concentrations of the solute. The lipid bilayer cooperativity was found to be higher in the confined systems compared to the liposomal systems despite the presence of higher disorder in the hydrophobic acyl chains in the former as suggested by lower main phase transition temperatures. The partition coefficient of BA within the bilayers of DPPC was found to be higher in liposomal systems in comparison to the confined systems. The differences in mean pore sizes of the micron sized silica did not result in any significant differences in the partitioning behaviour of BA within DPPC. The results helped us understand the partitioning of BA in systems in which DPPC was confined into silica nanopores relative to DPPC liposomes. The knowledge of the behaviour of boronic acid in confined systems can help us in designing biomimetic systems, with optimum concentrations of the embedded molecule, to serve the purpose of separation of compounds from dilute aqueous solutions.

Subsequently, the method of evaporation deposition was used to fill the pores of silica nanoparticles with 1,2-dipalmitoyl-sn-glycero-3- phosphocholine (DPPC) and assess the effect of increasing the mass ratio of lipid to silica nanoparticles on the zeta potential and colloidal stability of the nanoparticles. An increase in the mass ratio resulted in observable reductions in magnitudes of zeta potential of the resulting nanoparticles compared to bare silica nanoparticles. Lipid enveloping of pore filled silica nanoparticles results in zeta potentials comparable to that of DPPC liposomes. The reductions in zeta potentials of the lipid filled silica nanoparticles were hypothesized to be the result of several isolated lipid bilayers covering the exterior

surface of the nanoparticles, besides filling the nanopores. The complete assessment of colloidal stability of the system necessitates obtaining of information regarding the changes in hydrodynamic diameters and the settling behaviour, with extended time periods, of the lipid filled particles in conjunction with the obtained values of zeta potential of the system. The determination of the optimal amount of lipids that can be deposited into the silica nanopores would enable the designing of systems involving extraction and sensing of highly lipophilic molecules from dilute solutions.

Keywords: Silica nanoconfinement, 1,2-dipalmitoyl-sn-glycero-3- phosphocholine (DPPC), Differential Scanning Calorimetry (DSC), Boronic acid Partition coefficient, Zeta potential, Colloidal stability

Aniruddha Atul Shirodkar

April 24, 2020

## EFFECT OF SILICA NANOCONFINEMENT OF LIPID BILAYERS ON ITS PHASE TRANSITION AND ON THE COLLOIDAL STABILITY OF SILICA NANOPARTICLES

By Aniruddha Atul Shirodkar

Barbara L. Knutson, Ph.D

Co-Director of Thesis

Stephen E. Rankin, Ph.D

Co-Director of Thesis

Stephen E. Rankin, Ph.D

Director of Graduate Studies

April 24,2020

Date

#### ACKNOWLEDGEMENTS

The completion of this thesis would not have been possible without the invaluable assistance of many people. Firstly, I would like to thank Prof. Barbara Knutson for having guided me through every step during the three-year period. The inputs provided by Prof. Stephen Rankin from time to time were extremely instrumental in shaping up my research.

The camaraderic combined with the scientific and emotional assistance provided by my lab mates genuinely helped me go through this three-year grind. I would like to thank Dr. Shanshan Zhou for having introduced me to the relevant tools and techniques to get me started with the research process. I would like to thank Dr. Arif Khan, Dr. Yuxin He, Mahsa Moradipour, Joshua Garay, Rami Ghanim, Rebecca Pickman Pike, Andrew Drake and Sayma Afrin for all the help and the interactions we have had during this time period. Also, I would like to thank the students from all the other labs in the department who helped me getting acquainted with different instruments to execute my research. I would also like to acknowledge the efforts taken by the high school student McKenna Clinch for having shown immense focus and dedication to execute many experiments in this thesis.

I would also like to thank Nico Briot to have helped me get acquainted with the SEM and Dali Qian with the XPS. They have shown immense patience in trying to teach me these techniques.

I cannot really express how helpful the presence of my room mates (or rather good friends) Rishabh Shah and Lakshya Malhotra has been during this time period. They have really helped me emotionally through the difficult phases encountered during my research and pushed me to keep continuing in the hardest of times. Also, all my other friends in the city of Lexington (there are just too many to name!!) who have really made my time spent here worth reminiscing.

Finally, my parents! Expressing my gratitude towards them for having been a solid backbone in my life is the least that can be done and this is certainly not enough!! It is their guidance, combined with showering of immense love upon me, which has

moulded me into a person who I am today. Staying thousands of miles away in India, they were able to support me emotionally through this entire journey. Thank you so much Mumma, Baba and Nanu for everything!!

#### TABLE OF CONTENTS

ACKNO	OWLEDGEMENTS	iii
LIST OF	F TABLES	viii
LIST OF	F FIGURES	ix
Chapter	1: Background	1
1.1	Ordered mesoporous silica materials	1
1.2	Surfactant templating for ordered mesoporous silica	3
1.3	Lipid bilayers and its properties	7
1.4	Types of lipid bilayers investigated in this thesis	8
1.4.	1 Liposomes	8
1.4.2	2 Supported lipid bilayers	11
1.4.3	3 Pore-confined lipid bilayers	12
1.5	Differential Scanning Calorimetry(DSC) details	14
1.6	Zeta potential	16
-	2: Effect of nanoconfinement in silica pores and boronic acid incorphase transition of lipid bilayers	-
	Introduction	
	Experimental Section	
2.2.1	-	
2.2.2		
2.2.3		
2.2.4		
2.2.5	5 Fourier transform infrared spectroscopy (FTIR)	26
2.2.6	6 Preparation of liposomes containing boronic acid	27
2.2.7 thro	7 Boronic acid (BA) immobilized lipid filled silica particle prepugh evaporation deposition	
2.2.8	8 Confocal microscopy	28
2.2.9	9 Differential Scanning Calorimetry (DSC)	28
2.2.	10 Calculation of solute partition coefficient	29
2.3	Results and discussion	30
2.3.	1 Characterization of SBAS micron-sized silica	30
2.3.2	2 Characterization of lipid filled particles	33
2.4	Conclusion	45

-	r 3: Effect of lipid pore filling on the colloidal stability of mesoporous	
3.1	Introduction	
3.2	Materials and Methods	
3.2	2.1 Materials	51
3.2	2.2 Synthesis of spherical mesoporous silica particles	52
3.2	Materials Characterization using BET	52
3.2	2.4 Materials characterization using Scanning Electron Microscopy	<i>y</i> 52
3.2	Fourier transform infrared spectroscopy (FTIR)	53
3.2	2.6 Lipid filled silica particle preparation through evaporation depo	osition.53
3.2	2.7 DPPC liposome preparation	53
3.2	2.8 Preparation of lipid enveloped silica nanoparticles by vesicle fu	ısion 54
3.2	2.9 Analysis of zeta potential	54
3.3	Results and Discussion	55
3.3	.1 Characterization of mesoporous silica nanoparticles (MSNPs)	55
3.3	.2 Characterization of lipid filled particles	59
3.4	Conclusions	64
	lix A: Dye uptake studies of Sulforhodamine 101 within amine funct nesoporous silica nanoparticles.	
A.1	Introduction	66
A.2	Experimental section	67
A.2	2.1 Materials	67
A.2	2.2 Synthesis of radially oriented mesoporous silica nanoparticles .	67
A.2	2.3 Synthesis of amine functionalized mesoporous silica noparticles(MSNPA)	67
A.2 usii	2.4 Calibration curve for Sulforhodamine 101 dye uptake and dye ng amine functionalized silica nanoparticles	
A.2 fun	2.5 Solution depletion studies of Sulforhodamine 101 dye using an actionalized silica nanoparticles	
A.2 fun	2.6 Sulforhodamine 101 dye release quantification from amine actionalized silica nanoparticles	68
A.3	Results and Discussions	69
Append	lix B: Attachment of acryl-modified DNA onto thiol attached glass co	verslips
B.1	Introduction	
B.2	Experimental section	73
R 2	7.1 Materials	73

B.2	2.2	Cleaning of glass coverslips	74
B.2	2.3	Thiol modification of glass coverslips	74
B.2	2.4	DNA attachment to thiol attached glass coverslips	74
		Analysis of thiol attachment and DNA attachment using X-ray ectron spectroscopy (XPS)	74
B.3	Res	sults and Discussion	75
Referen	ices		83
VITA			96

#### LIST OF TABLES

Table 1:Stability behavior of colloids based on zeta potential values. Reproduced with
permission from Kumar, and Dixit [89]
Table 2: Surface area and pore size distribution of SBAS micron-sized silica31
Table 3:A summary of various parameters obtained of the DSC thermograms for: (a)
DPPC liposomes
Table 4:A summary of various parameters obtained of the DSC thermograms for BA
incorporated DPPC bilayers confined in SBAS micron-sized silica nanoparticles of
mean pore size of 7.4 nm39
Table 5:A summary of various parameters obtained of the DSC thermograms for BA
incorporated DPPC bilayers confined in SBAS micron-sized silica nanoparticles of
mean pore size of 11.7 nm40
Table 6: Table determining the results of the linear regression of Equation 2.1. The
slope M is calculated using Equation 2.2. In the table, BA in SBAS-90 denotes boronic-
acid incorporated DPPC micron-sized silica synthesized at 90°C and having mean pore
size of 7.4 nm; BA in SBAS-110 denotes boronic-acid incorporated DPPC micron-
sized silica synthesized at $110^{\circ}\text{C}$ and having mean pore size of $11.7$ nm. $K_{\text{m/w}}$ denotes
the octanol-water partition coefficient
Table 7: Surface area and pore size distribution of MSNPs    57
Table 8:Zeta potential of various MSNPs. In the above figure, LE MSNPs refers to
lipid enveloped MSNPs; LPx MSNPs refer to lipid filled silica nanoparticles, where x
equals 1,2,3 refers to lipid to silica nanoparticle mass ratios of 1:1,2:1 and 3:1
respectively;LP1 LE MSNP refers to lipid filled silica nanoparticles with 1:1 mass ratio
of lipid to silica nanoparticle with an enveloping of DPPC vesicles. The measurements
are taken in PBS solution, containing 137mM of sodium chloride, 2mM of potassium
chloride and 10mM of phosphate buffer64

#### LIST OF FIGURES

<b>Figure 1:</b> An illustration of the hydrolysis and condensation reactions involved in solgel synthesis. Note that only one of up to four reactive Si-OR or Si-OH groups is shown.
Figure 2:(a)Overview of a synthetic approach to the mesoporous silica formation by assembly of surfactants into micelles followed by addition of silica precursors to form
a mesostructured network Removal of the surfactant template leads to a mesostructured
porous silica material. Adapted from Swar, S. et al. [25]. ;(b) Overview of a synthetic
approach to the mesoporous silica formation by nucleation and growth of seeds
followed by addition of silanol monomers and the orientation of surfactant
micelles(brown in color) at the silica -solution interface. Removal of the surfactant
template leads to a radially oriented mesostructured porous silica material. Adapted
with permission from Han, Y., et al [6].
Figure 3:Illustration of a typical biological membrane. (a) In the absence of membrane
proteins, minimum to no transport;(b) In the presence of membrane proteins, transport
of nutrients occurs.
Figure 4:(a) Schematic of pore confinement of DPPC within silica nanopores. Adapted
from Zhou et al.[43]; (b) Lipid diffusivity as a function of pore size and the position within the pore. The figure is reproduced with permission from (Schlipf et al.[52])14
Figure 5:Schematic of the heat-flow Differential Scanning Calorimetry (DSC) 16
<b>Figure 6:</b> A schematic of the electric layer of the surface of silica nanoparticles. Below,
the graph of surface potential with respect to the distance of the particle from the
surface. The image is adapted with permission from Selvamani, Vijayakumar[72]20
Figure 7:Scanning electron microscopy (SEM) image of SBAS micron-sized silica of
mean pore size 7.4 nm, synthesized at 90 °C
Figure 8: (a) Pore size distribution of SBAS micron sized particles prepared at 90°C
and 110 °C; (b) Adsorption isotherm of SBAS micron-sized particles32
Figure 9: FTIR spectra of SBAS micron-sized silica particles mean pore size 7.4 nm,
synthesized at 90 °C.
Figure 10:Confocal microscopy image of boronic acid incorporated lipid filled silica
nanoparticles. The red colour is due to the ARS-BA complex formation. The SBAS
micron-sized silica particles have a mean pore size 7.4 nm and synthesized at 90 °C.
BA (1% by weight of DPPC) was incorporated in 20mg of DPPC along with 10 mg of
SBAS micron-sized silica and ARS was used
Figure 11: DSC thermograms of: (a) DPPC liposomes with boronic acid incorporated
from 0 weight percent to 4 weight percent; (b) DPPC bilayers confined within the pores
of micron-sized silica (7.4 nm pore diameter) with the incorporation of boronic acid
within the bilayers 0 weight percent to 4 weight percent; (c) DPPC bilayers confined
within the pores of micron-sized silica (11.7 nm pore diameter), with the incorporation
of boronic acid within the bilayers from 0 weight percent to 4 weight percent39
Figure 12: Melting point depression of DPPC upon boronic acid addition from 0 weight
percentage to 4 weight percentage in : (a) Liposomal systems (blue); (b) boronic-acid incorporated DPPC micron-sized silica synthesized at 90 °C (BA-DPPC 90); (c)
boronic-acid incorporated DPPC micron-sized silica synthesized at 110°C (BA-DPPC
110)
Figure 13:Scanning electron microscopy (SEM) image of MSNPs

Figure 14:(a) BJH pore size distribution of MSNPs calculated using t	the adsorption
branch of the nitrogen adsorption isotherm; (b) nitrogen adsorption a	and desorption
isotherm of MSNPs. The blue points represent the adsorption isotherm a	and the orange
points represent the desorption isotherm.	58
Figure 15:FTIR spectrum of MSNPs in a KBr pellet	58

#### **Chapter 1: Background**

#### 1.1 Ordered mesoporous silica materials

Metal oxide nanoparticles are often synthesized by a process called the sol-gel process because this method allows excellent control of particle size, pore size distribution and morphology by systematic tuning of reaction parameters.[1]. The steps involved in the synthesis are hydrolysis, followed by condensation, formation of a solid matrix (by gelation or precipitation), aging, and drying[2] (See Figure 1 below). The process of hydrolysis usually involves nucleophilic attack of alkoxide precursors by water molecules in either acidic or basic media. The hydrated silica molecules subsequently participate in condensation reaction with other silica molecules to form a three-dimensional gel network. The condensation of silica molecules leads to the formation of nucleation of clusters which could then grow by addition of small oligomers or aggregate in solution depending on the balance of colloidal forces[2]. Depending on the synthesis conditions (especially pH), a sample-spanning gel or dispersed particles may be the product. The process of aging serves to continue with the polycondensation of silica species with a concomitant increase in the strength of the gel [3]. The density and viscoelastic properties of this gel are greatly dependent on the particle size and the extent of cross-linking. Hydrolysis and condensation reactions are acid and base catalysed, and are generally thought to proceed by substitution reactions, although several viable detailed mechanisms have been proposed. (See Figure 1 for the illustration of the reactions). Since the Chapter 2 of the thesis involves formation of micron-sized silica nanoparticles with an acidic catalyst, an explanation of the fundamental mechanisms involved is relevant. When hydrolysis involves catalysis by acidic groups, the alkoxide bond is protonated and the rate determining step is found to

be the nucleophilic addition of the water molecule, onto the silicon atom, which acquires a partial positive charge due to the electron cloud shifting towards the protonated oxygen in the alkoxide molecule, followed by the subsequent departure of the alcohol molecule[4]. This reaction is also found to be first order with respect to the concentration of water in those acidic conditions. The condensation progresses by the attack of hydronium ion onto the silanol group followed by the formation of a siloxane bond between the protonated and unprotonated silanol groups [5]. In Chapter 3, the formation of silica nanoparticles occurs via a base-catalyzed mechanism. Generally, the rate of hydrolysis in such a system is increased with an increase in concentration of the base. The Si atom in this case is attacked by a more nucleophilic hydroxyl ions. The process of condensation between the hydroxyl ions of two silanol groups or ethoxyl groups, formed during hydrolysis, takes place again in the form of a nucleophilic attack by the hydroxyl ions [6].

**Figure 1:**An illustration of the hydrolysis and condensation reactions involved in solgel synthesis. Note that only one of up to four reactive Si-OR or Si-OH groups is shown. Adapted from Righini, Giancarlo C., and Andrea Chiappini.[7]

#### 1.2 Surfactant templating for ordered mesoporous silica

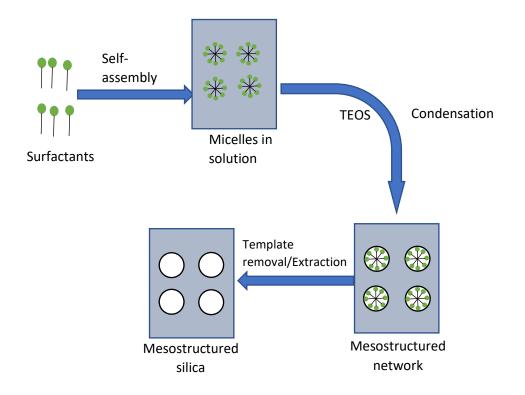
Templating, in the case of formation of mesoporous silica nanoparticles, is the process by which an organic species co-assembles with inorganic oxide-based moieties resulting in the formation of an ordered structure[8]. The organic species, a surfactant in this thesis, is also called a Structure Directing Agent (SDA)[9]. Self-assembly of surfactants occurs above their critical micelle concentration (cmc) and results in the formation of cylindrical or spherical micelles. A further increase in the concentration leads to formation of various mesophases such as lamellar, hexagonal, cubic, for example. [10]. The interactions occurring between the inorganic (silica precursors) and the organic (surfactant) species is dependent on the pH of the medium. A pH of the medium above the isoelectric point (IEP) (above pH 2.0) of the silica results it being negatively charged, thereby providing a driving force for co-assembly with either

positively charged or neutral surfactants via electrostatic or hydrogen bonding interactions, respectively[11]. (See **Figure 2** for the templating mechanism). The removal of the SDA results in the formation of an ordered porous structure in which the geometry and connectivity of the self-assembled organic species are retained by the inorganic matrix[12].

Generally, nanoparticle synthesis involves creation of several nuclei followed by growth. Independent occurrence of these steps could be desirable so as to prevent a broad particle size distribution due to multiple nucleation events. The occurrence of agglomeration of nanoparticles is highly probable and its reduction is necessary for a stable colloidal solution of silica nanoparticles [13]. Pluronic F127, a non-ionic triblock copolymer, for example, can be used to prevent agglomeration by attaching itself to cationic surfactant-silica complexes, thereby arresting further particle growth leading to narrowly distributed 50 nm diameter particles [14]. The Stöber method, in which tetraalkyl silicates are hydrolysed in a solution containing ethanol and ammonia as a catalyst, is one of the effective methods used to synthesize monodisperse silica nanoparticles[15]. Since its initial development, various modifications have been made, which involve inclusion of surfactants[16, 17], changing solvent compositions[18] etc. One of the proposed mechanisms involved in generating mesoporous materials involves initial formation of clusters by hydrolysis and condensation of silanol monomers of tetraalkyl silicates, followed by reaction of remaining silica precursors upon existing silanol groups on the surface of silica nanoparticles[6]. The latter step could be contributing towards the generating high levels of monodispersity among the nanoparticles. The pore formation, as we have discussed above, requires the presence of surfactants. Several researchers have found that the organization of surfactant micelles occurs radially at the interface of the silica nanoparticles formed[2, 19, 20]. It

is hypothesized by some researchers that the radial orientation of the micelles begins at the Ia3d cubic (MCM-48) seeds[21, 22]. However, there has also been evidence suggesting that cubic seed formation does not take place and that emanation of radial orientation takes place from the surface[2].

The control of pore size of the nanoparticles has been found to be influenced by many factors, which include increasing the chain length of the SDA or by the addition of an auxiliary molecule such as 1,3,5-trimethylbenzene which solubilize at the hydrophobic core of the SDA thereby leading to an increase in the micellar diameter[23]. It has been found that larger micelles (achieved using larger SDAs or micelles swollen with additives) leads to larger self-assembled structures (for example, larger micelle molecules or micelles swollen with additives)[24]. Aging at elevated temperature has also been shown in some systems to lead to the increases in pore size. For example, in the case of silica nanoparticle synthesis involving a non-ionic polyethylene oxide (PEO) block and alkoxide silica precursor, an increase in temperature is believed to weaken the hydrogen bonding between them. This causes the size of the head group of the micelles to decrease, causing the reduction in the micellar curvature. The increasing temperature will also lead to the increase in the size of the hydrophobic portion of the micelles, which ultimately determines the pore size of the nanoparticles formed [25]. This phenomenon of micelle swelling by hydrothermal aging is used in Chapter 2 of this thesis to synthesize Santa Barbara Amorphous material (SBA) Spheres (SBAS) with a 5-10 micron particle size and pore sizes of 5-12 nm diameter by varying temperatures from 60 to 120 °C.



(a)

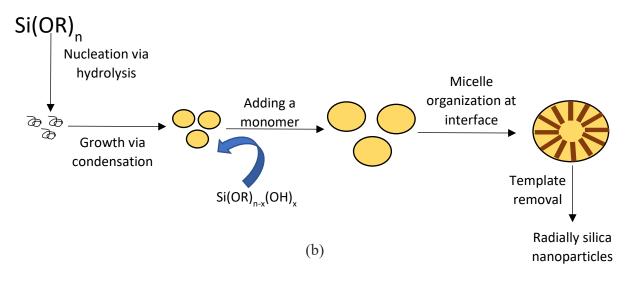
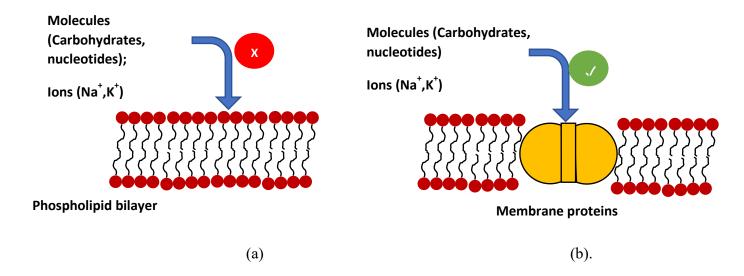


Figure 2:(a)Overview of a synthetic approach to the mesoporous silica formation by assembly of surfactants into micelles followed by addition of silica precursors to form a mesostructured network Removal of the surfactant template leads to a mesostructured porous silica material. Adapted from Swar, S. et al. [26]. ;(b) Overview of a synthetic approach to the mesoporous silica formation by nucleation and growth of seeds followed by addition of silanol monomers and the orientation of surfactant micelles(brown in color) at the silica -solution interface. Removal of the surfactant template leads to a radially oriented mesostructured porous silica material. Adapted with permission from Han, Y., et al [6].

#### 1.3 Lipid bilayers and its properties

Biological membranes play an important role in controlling the transport of ions and nutrients into cells[27]. In general, they are composed of complex mixtures of lipid bilayers, solvation modifiers such as cholesterol, and proteins. The lipid bilayers, which are a "two-dimensional fluid" [28] within the membrane, are self-assembled structures of lipid molecules with consist of hydrophilic head groups and a hydrophobic tails. There is a spontaneous arrangement by which the hydrophobic tails are shielded from the water molecules and the hydrophilic heads are exposed to the water molecules [29]. The lipid bilayer acts as a barrier to the flow of many molecules such as water, ions and other aqueous solutes by ensuring that only a limited amount of them pass through the cell membrane[30]. The presence of carrier proteins and channel proteins incorporated within the bilayer allows for controlled transport of molecules such as carbohydrates and ions such as Na<sup>+</sup>, K<sup>+</sup> across the membrane[31]. (See **Figure 3** for an illustration of a lipid bilayer membrane). This system is being mimicked in Chapter 2 by incorporating boronic acid into bilayers of 1,2-dipalmitoyl-sn-glycero-3- phosphocholine (DPPC) bilayers to bind and transport carbohydrates. Such a system has been previously

experimented with by Zhou et al. [32] to observe the permeability of solutes such as glucose, xylose and cellobiose through the bilayers



**Figure 3:**Illustration of a typical biological membrane. (a) In the absence of membrane proteins, minimum to no transport;(b) In the presence of membrane proteins, transport of nutrients occurs.

#### 1.4 Types of lipid bilayers investigated in this thesis

#### 1.4.1 Liposomes

Liposomes are spherical vesicles consisting of one or more bilayers which separate an internal aqueous solution core from an external medium [33]. The method of preparation of liposomes can be adjusted to obtain liposomes of different size and number of lipid bilayers. If a dry lipid film is hydrated in a vigorous manner at a temperature which lies above the phase transition of the lipid, we normally expect to get multilamellar lipid vesicles (MLVs). These are characterized by several concentric lipid bilayers and they display a range of sizes from 0.5-10 µm [34]. Large unilamellar

vesicles (LUVs) of sizes varying from 100 nm to 500 nm are obtained upon extrusion of MLV's through a porous polycarbonate membrane [35]. In this thesis, we will be making liposomes of sizes less than 200 nm, which will be generated upon extrusion of liposomes through polycarbonate filters. On the other hand, small unilamellar vesicles (SUV's) exhibiting diameters lesser than 50 nm are obtained upon sonication of MLV's in either a bath-type sonicator or a probe sonicator [36]. Traditionally, liposomes are used as drug delivery agents due to several favourable properties which include: low toxicity, several possible routes of administration, their ability to encapsulate wide variety of drugs, and the possibility of surface modification for biocompatibility or targeting[37, 38]. The stability of liposomes is affected by several factors such as hydrolysis due to buffer species. The presence of a buffer species is usually found to speed up the process of hydrolysis, which is usually attributed to the presence of protons and hydroxyl ions[39]. The changes in liposome sizes due to processes such as aggregation and fusion is strongly dependent on the composition of the medium and the pH[40, 41] [42]. In this thesis, the liposomes of DPPC have been synthesized using polycarbonate filters of 200 nm pore diameter and are dispersed in a Phosphate Buffer Saline (PBS, pH 7.4).

With regards to the stability of the DPPC liposomes, Armengol and Estelrich[42] reported that the polydispersity index (PDI) of unilamellar vesicles, which is an indication in this case of the extent of aggregation of the liposomes under study, increased to more than twice its original valueupon keeping the liposomes at room temperature for close to seven days. However, at 50 °C, which is above the main phase transition of the lipid, the jump in PDI to twice the value took more than 30 days. The presence of cholesterol resulted in prolonged stability by ensuring lower tendencies to aggregation. However, in this thesis, we carry out the experiments on liposomes on the

same day, obviating any concerns about issues with excessive liposomal aggregation. Since the Chapter 2 of this thesis partly involves incorporation of phenylboronic acid (BA) in liposomes of DPPC, it is important to have an idea about how stability of liposomes in the presence of solutes within the bilayer affects its stability. In the case of introduction of  $\alpha,\beta,\gamma$  cyclodextrins(CD), the mean size of DPPC vesicles, in the presence of CD at a molar ratio of 7:1 of CD to DPPC liposomes, resulted in between 2.5-20 fold increase in the size compared to DPPC vesicles [43]. However, introduction of polymers which are derivatives of polyvinyalocohol (PVA) were shown to reduce the extent of aggregation of vesicles. However, the aggregation was observed for a period of 20 days and there was no noticeable change in vesicle sizes for a period of one day, except for α-CD's . It is also important to know the extent of leakage of embedded carrier molecule in the presence of an external medium. It is desirable to ensure minimum leakage of the carrier medium so as to improve the transport properties[44]. In this regard, the research done by Kokkona, Maria, et al.[45] demonstrated that the release of carboxyfluorescein (CF),embedded in DPPC liposomes, was dependent on the composition of the medium (pancreatin, 10 mM sodium cholate and 10 mM sodium taurocholate). The release in most cases was around 40% for pancreatin and 80-100% for sodium cholate and sodium taurocholate for an incubation period between 0-5 hours. However, the presence of cholesterol in the DPPC matrix was found to drastically reduce it to levels below 40%. However, boronic acid is shown to be extremely lipophilic in DPPC and is shown to be miscible with the lipid bilayers and the presence of additives to ensure minimum leakage of the molecule was not required[44].

#### 1.4.2 Supported lipid bilayers

A supported lipid bilayer (SLBs) consist of a planar lipid bilayer which is supported on a solid surface like mica, glass[46]. The hydrated polar head groups of the first monolayer of the lipid are in contact with the solid support and the hydrocarbon chains of the same monolayer come in contact with the chains of the second monolayer[27]. One of the mechanisms if formation of SLBs, called vesicle fusion, involves the adsorption or fusion of the lipid vesicles on the surface, which is then followed by their deformation, flattening and rupture[47]. Some of the advantages enjoyed by the SLBs over liposomes are their increased stability and easier characterization by a variety of surface techniques in comparison to free-floating vesicles[48]. One of the major drawbacks of using such systems is the closeness of the incorporated molecules and the solid surface, thereby leading to issues with mobility of the components embedded within the membrane. Tethered lipid bilayers are sometimes used to circumvent this problem. In this system, there is either a layer or a spacer molecule lying in between the lipid bilayer and the solid support. This is usually achieved by different methods such as addition of a polymer film, self-assembled chemically-modified lipids on solid surface, spacer lipid fusion on surfaces [49]. The preparation of SLBs on mesoporous silica supports has been one of the techniques investigated to ensure incorporation of molecules such as proteins within the lipid bilayer matrix [50-52] Additionally, such an arrangement also permits the ability to access the internal pore volumes from the surface of the lipids[50]. Compared to nonporous surfaces, SLBs on mesoporous supports have an added benefit of the presence of enhanced fluidity of bilayers[43]. However, pore confined lipid bilayers, which are discussed in Section 1.4.3, offer an added advantage compared to traditional supported bilayers due to higher resistance observed to the uncontrolled flow of molecules, which

is a critical requirement for carrier mediated transport through biomimetic membranes [32]

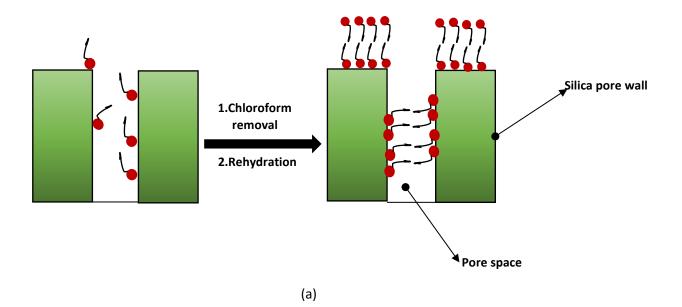
#### 1.4.3 Pore-confined lipid bilayers

The confinement of DPPC lipid bilayers into pores of silica nanoparticles was carried out by Schlipf et al.[53] and Zhou et al. [32] using the method of evaporation deposition. This involves addition of lipid molecules into the pores of silica nanoparticles using chloroform as a solvent. The lipid can be deposited within the pores by removing the organic solvent through the application of vacuum. Lipid assemblies then are formed in the pores by subsequently carrying out rehydration.

The experiments conducted by Schlipf et al. [53] demonstrated the incorporation of DPPC lipid bilayers within mesoporous particles with pore diameters of 5.4 and 9.1 nm (see Figure 4(b)) However, at a pore diameter of 3.0 nm, the lipid only formed at the surface of the silica nanoparticles (see Figure 4(b)). Also, diffusivity values were measured by fluorescence recovery after photobleaching (FRAP) and found to be similar both at the surface and inside the pores of lipid-filled particles. The results show that the there is no significant effect on lipid mobility upon pore confinement compared to that on the surface of the particles.

Zhou et al. [32] used this system to measure the permeabilities of compounds, consisting of glucose, xylose and cellobiose, through a membrane system consisting of boronic acid incorporated within the DPPC bilayers filled within pores of silica membranes deposited on aluminium oxide supports. Boronic acids have been used extensively in research applications as carrier molecules for separation and sensing [54] of molecules such as glycoproteins [55, 56] and saccharides [57] due to their ability to form reversible covalent bonds with 1,2- and 1,3-diols by accepting a lone pair of

electrons from Lewis bases [58]. The parameters such as pH and temperature of the system were varied and the permeability of the molecules measured. Specifically, the permeabilities of the compounds at 59 mol% of boronic acid with respect to DPPC was investigated. However, this concentration was found to nearly eliminate the main phase transition of DPPC. It is desirable to incorporate boronic acid in lesser amounts such that main phase transition of DPPC, involving rearrangement of lipid bilayers from gel to fluid phase, is existent. In this thesis, boronic acid is incorporated in smaller amounts, from 0 to 7 weight percentage (0 to 20 mole percentage) with respect to amount of DPPC, within DPPC bilayers confined within pores of micron-sized silica nanoparticles and liposomes of DPPC. The thermal phase transitions of the resulting samples will be analysed using Differential Scanning Calorimetry (DSC) discussed in Section 1.5. For pure DPPC liposomes, the value of the main phase transition temperature is found to be around 42.5°C[59, 60]. From the depression of the main phase transition temperature, we determine the differences in partitioning coefficient of boronic acid within DPPC in the form of liposomes and confined in nanopores of micron-sized silica nanoparticles.



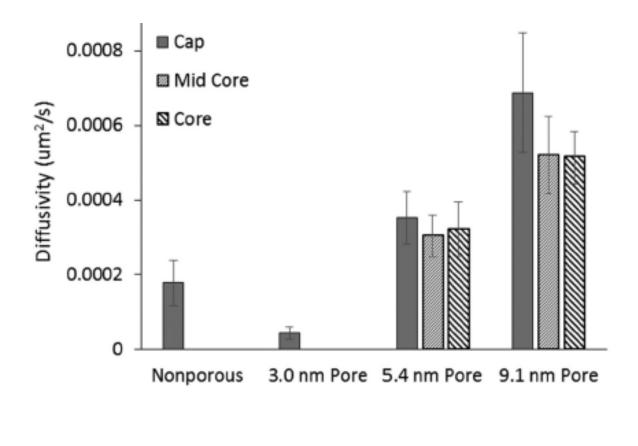


**Figure 4:(**a) Schematic of pore confinement of DPPC within silica nanopores. Adapted from Zhou et al.[44]; (b) Lipid diffusivity as a function of pore size and the position within the pore. The figure is reproduced with permission from (Schlipf et al.[52]).

(b)

#### 1.5 Differential Scanning Calorimetry(DSC) details

Differential Scanning Calorimetry (DSC) has been widely used, for instance for biological molecules like lipids and proteins, to measure thermodynamic properties which arise due to phase transitions occurring due to application of heat [61, 62]. In general, a DSC unit consists of a sample cell and a reference cell. In a power compensation unit, the temperature in both cells is independently controlled and monitored by ensuring a steady rate of increase of temperature. At a thermal transition temperature, the sample cells require more or less heat in comparison to the reference cell to maintain the same cell temperature. The difference in the heat required is used

to measure the heat flow[63]. In the heat flux DSC, both the sample and reference cells are connected to a heat flow circuit such as a metal disk and the temperature of both the cells is varies linearly with respect to time. However, at a thermal transition temperature, the temperature of the reference cell continues to increase in comparison to the sample cell. To maintain the same temperature of the sample cell, extra heat flux is required by the sample cell to match the temperature of the reference cell. The heat of a phase transition is measured as a peak (either endothermic or exothermic) on the DSC thermogram[64]. (See **Figure 5** below for the schematic of the DSC)

Here, DSC is used to investigate thermal transitions in lipid bilayers in vesicles, at the surface of particles, or confined within nanopores. In lipid bilayers, two phases which are usually found are the gel and the fluid phases. In the gel phase  $(L_{\beta}, \text{ or } L_{\beta})$ , also known as the solid-ordered (S<sub>0</sub>) phase, there is an ordered hexagonal [65] arrangement of lipids. It is also a phase in which low lipid mobility is observed due to the van der Waals interactions between the hydrocarbon chains, thereby leading to a highly ordered packing of the lipids [66]. The fluid phase or the liquid-disordered ( $L_{\alpha}$  or L<sub>d</sub>) phase is commonly associated with higher molecular mobility in comparison to the gel phase, thereby resulting in increased fluidity of the cell membrane [67]. The temperature at which such a transition occurs from the gel phase to the fluid phase is termed as the thermotropic phase transition temperature (T<sub>m</sub>), which is usually determinable using the DSC technique and is largely dependent on the nature of the acyl chains of the lipid bilayers[68]. In the case of phosphatidylcholines, there exists a transition termed as the pre-transition temperature, which lies a few degrees below the main phase transition. This pre-transition during heating results in some degree of ordering of the lipid chains to form a ripple phase[69] from a flat membrane and is dependent on the interactions between the lipid head groups and the solvent surrounding them[70]. In this thesis, we will explore the changes in main phase transition temperatures of the lipid 1,2-dipalmitoyl-sn-glycero-3- phosphocholine (DPPC) upon confinement in pores of silica nanoparticles using this technique. The confinement of DPPC will result in possible interactions between the silica surface and the polar head groups of DPPC, which could result in the temperature shifts. Also, the shift in main transition temperatures upon addition of a boronic acid derivative into DPPC bilayers will be measured. The addition of boronic acid is expected to cause a disruption in the hydrophobic acyl chains of DPPC, thereby leading to a possible shift in the temperature at which the gel phase of the lipid transforms into a fluid phase phase.

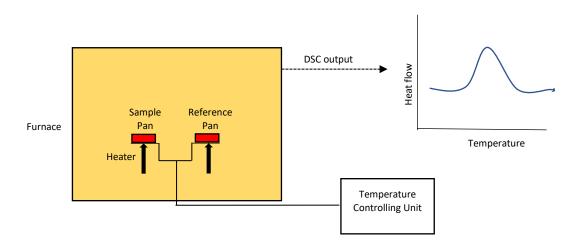


Figure 5: Schematic of the heat-flow Differential Scanning Calorimetry (DSC).

#### 1.6 Zeta potential

Zeta potential measures the potential difference between the medium of a dispersion and the stationary layer of fluid close to the particle surface [71, 72]. The stationary layer contains ions which have a charge which is opposite to that of the surface of the particles with which they are associated [73]. The layer which is in direct association with the surface of the particles is termed as the Stern layer, which is further

surrounded by ions loosely attached to the Stern layer called the "diffuse ion layer". These layers form an electric double layer (EDL). The boundary between the strong interactions ions in the diffuse layer and that in the bulk is called the slipping plane[74]. The potential at the surface of the particle is called the surface potential and at the slipping plane is the zeta potential. The surface potential keeps reducing in magnitude as the distance from the surface increases. The researchers sometimes also refer to the potential at the Stern layer as the zeta potential[75]. See **Figure 6** below for a schematic of the electric layer on the particle surface.

When an electric field is applied to the particle dispersion, the charged particles move towards the oppositely charged electrode. The zeta potential is deduced by measuring the electrophoretic mobility ( $\mu_e$ ) of charged particles under the application of this electric field. This is calculated using the knowledge of the particle velocity and the strength of the electric field. The particle velocity is determined using Dynamic Light Scattering (DLS). In this case, the laser incident on the mobile particles has a frequency which is different from the original frequency. This shift in the frequencies is proportional to the velocities of the particles. If the size of the EDL is much smaller in comparison to the particle radius, then the zeta potential is calculated based on the Helmholtz-Smoluchowski (HS) equation, which is given below:

$$\mu_{\rm e} = \frac{\varepsilon_r \varepsilon_0 \zeta}{\eta}$$
 (Equation 1)

where  $\varepsilon_r$  = relative permittivity/dielectric constant,  $\varepsilon_0$  = permittivity of vacuum,  $\zeta$  = zeta potential, and  $\eta$  = viscosity at experimental temperature[76].

Zeta potential is a widely used property for determination of the surface charge of nanoparticle dispersions [73, 77], which is in turn related to their stability in suspensions [78]. Generally, if  $\zeta$  is more than 30 mV or less than -30 mV, the particles

are considered to be electrostatically stabilized in a suspension [79, 80]. **Table 1** lists general guideline for how the zeta potential values correlate with particle stability when dispersed particles are not indefinitely stable. For charged particles, stability against van der Waals attractive forces comes from repulsive forces due to the presence of a charges of the same sign on the surface of the nanoparticles [81]. The zeta potential, and thereby the colloidal stability of the particles can be changed by varying pH and the ionic strength of the solution[79]. Increasing ionic strength by salt (such as NaCl) addition is known to cause aggregation of silica nanoparticles beyond a certain threshold concentration [82]. The hydroxyl-terminated surfaces of oxides such as silica are amphiprotic, gaining protons at low pH to form Si-OH<sub>2</sub><sup>+</sup>, and losing protons at high pH to form Si-O<sup>-</sup>. With an increase in pH of the solution above the isoelectric point (pH of 2-4 depending on the preparation route) of the silica nanoparticles, they become more negatively charged. This leads to a corresponding negative zeta potential of the nanoparticles [83].

Typical values of zeta potentials reported in literature for silica nanoparticles in solutions containing low concentrations of NaCl are around -45 mV[84-86]. Also, the concentration and the type of the electrolyte used could also destabilize particle dispersions by reducing the thickness of the electrical double layer. An addition of different type of salts such as NaCl, CaCl<sub>2</sub>, MgCl<sub>2</sub>, and BaCl<sub>2</sub> causes aggregation of silica nanoparticles [84]. There have been some studies conducted on assessing the effects of ionic strength, pH and the ratio of amount of lipid to silica nanoparticles on their colloidal stability[86-88]. In a set of experiments carried out by Moura and Carmona-Ribeiro [86] on deposition of zwitterionic phospatidylcholine (PC) bilayers on silica nanoaprticles, it was found that a higher ionic strength promotes an increase in affinity of the PC vesicles for the particles. The resulting zeta potentials were reduced

in magnitude compared to the bare silica nanoaprticles. However, no significant settling of particles was observed even after 48 hours at an ionic strength of 150mM. The stabilization of PC enveloped silica nanoparticles is a possible consequence of the presence of hydration forces which are more dominant than the electrostatic repulsive forces at particle separations within 20 Angstroms and is found to be a very significant force especially for two zwitterionic lipid bilayers coming close together[89]. In this thesis, we will be analysing the effect of lipid filling within 8 nm on the zeta potential of silica nanoparticles in comparison to bare mesoporous silica nanoparticles, with a goal of interpreting their colloidal stability.

**Table 1:**Stability behavior of colloids based on zeta potential values. Reproduced with permission from Kumar, and Dixit [89]

Zeta potential value(mV)	Stability Behavior	
0 to ±5	Flocculation or coagulation	
$\pm 10 \text{ to } \pm 30$	Incipient stability	
±30 to ±40	Moderate Stability	
±40 to ±60	Good stability	
Greater than ±60	Excellent stability	

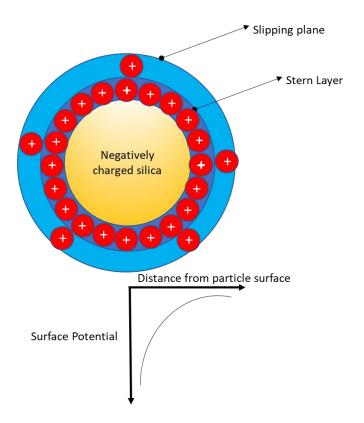


**Figure 6:**A schematic of the electric layer of the surface of silica nanoparticles. Below, the graph of surface potential with respect to the distance of the particle from the surface. The image is adapted with permission from Selvamani, Vijayakumar[73]

### Chapter 2: Effect of nanoconfinement in silica pores and boronic acid incorporation on the phase transition of lipid bilayers

#### 2.1 Introduction

Mesoporous silica nanoparticles have received immense attention over the recent years[90-92]. Their advantages for applications in separation, catalysis, and biomolecule loading are their uniform and tunable pore sizes [93], large surface areas and pore volumes [94]. This has led to its utilisation for several applications such as drug delivery and biomedical [95, 96], and biosensing [97]. Lipid bilayers coated on the surfaces of silica nanoparticles have been used as nanocarrier systems due to their improved biocompatibility and biological functionality [98]. Lipid coated particles are supported lipid systems, which are formed on the surfaces by the process of rupturing of lipid vesicles assisted by the presence of electrostatic interactions between the lipids and the hydrophilic silica nanoparticles[99]. The enhanced biological functionality of such systems is a result of the amphiphilic nature of the lipid bilayers enabling the encapsulation of both hydrophilic and hydrophobic components into the bilayer environment [98]. Also, the ability of the lipids to self- assemble into structures mimicking the biological cell membranes provides the motivation to develop biomimetic membrane models[100]. Much research has taken place involving loading of molecules into nanopores, followed by a lipid coating so as to enhance uptake of silica nanoparticles by cells in the body [101, 102]. Fluorescent lipid coated nanoparticles can be used in target specific cells for molecular imaging and cell tracking[103].

The effect of confinement of molecules within pores of mesoporous materials has been explored by several groups [104]. Various authors demonstrate increased rates

of reaction occurring within pores with dimensions closer to that of the molecule size, for example, the oligomerization of 1-butene[105] or acetalization of cyclohexanone with methanol [106]. Transition metal oxides, which find applications in energy conversion and storage, catalysis, sensing, adsorption and separation [107], have been found to attain stability within the channels of SBA-15 silica nanoparticles after executing a controlled one-pot synthesis of mesoporous silica nanoparticles involving block copolymers (surfactants), silica precursor tetraethyl orthosilicate and the corresponding metal nitrites of the transitional oxides. This is followed by the calcination and pyrolysis to remove surfactants and metal nitrite. The stability is thought to be a result of the favourable interactions between the -O- group of the block copolymers and the metal ions in the process of self-asssembly [108]. The pore functionalization of silica nanoparticles has shown to result in increased immobilization of enzymes due to the presence of hydrogen bonding between the silanol groups and the enzymes. The confinement also results in high levels of stability to external stimuli such as increases in temperature compared to free enzymes[109].

The changes in melting point, upon confinement into pores of silica nanoparticles, has been explored by several researchers for various molecules such as drugs and ionic liquids compared to their unconfined molecular state [110-113]. Differential Scanning Calorimetry (DSC) has been used to quantify these thermotropic properties[112, 114, 115]. For example, the loading of a poorly water-soluble drug carbamazepine into nanopores of SBA-16 resulted in the reduction of endothermic melting peak compared to its free form. A similar reduction, for a drug Rufinamide, was attributed to the restriction in the crystalline structure of the drug due to reduced pore sizes [116]. In contrast, in the case of ionic liquids, confinement into nanopores has shown to result in increase in melting points [113] [117] [118, 119] for some cases

and decreases for others[120-122]. This is controlled by the interactions between the cations and anions present in the liquid [117]. For example, the assembling of the ionic liquid [Emim]Br within the pores leads to its compression. This leads to an increase in the coulombic forces of attraction between the C-H cation and the Br anion, thereby resulting in stabilization and a corresponding increase in melting point [118]. The melting points of ionic liquids are also found to be pore size dependent, as evidenced by the experiments conducted on pore confinement of [Emim]Br within porous silica nanoparticles having pore sizes of 3.7 nm and 7.1 nm. The melting points were observed to be 88°C and 105 °C, respectively, relative to a melting temperature of 83°C in the bulk environment [113]. With regards to the depression in melting point of ionic liquids upon confinement in nanopores, it was found that the confinement of ionic liquid tributylhexadecylphosphonium bromide (P44416Br) within silica nanoparticles of average pore size of 3.7 nm resulted in the depression of melting point by around 8°C in comparison to its bulk form[122]. In general, the depression is attributed to the decrease in mobility of the cations at the interface upon confinement

Boronic acids have been used extensively in research applications as carrier molecules for separation and sensing [54]. They form reversible covalent bonds with 1,2- and 1,3-diols by accepting a lone pair of electrons from Lewis bases [58]. This property of boronic acids has been used for separations of wide class of compounds such as glycoproteins [55, 56] and saccharides [57]. The ability of carrier molecule to remain localized in the medium in which it is embedded is of immense importance during separation applications. Boronic acids, incorporated into liquid membranes, have been used by several researchers to demonstrate transport and separation of saccharides [31, 123, 124]. However, the carrier has been shown to leach out of the membranes into the aqueous phase, resulting in low sugar fluxes [124, 125]. The use of

lipid bilayers or liposomes for separations has first been reported for metal ion separations [126] and protein purification [127]. Smith [128] subsequently investigated the use of boronic acid in liposomes for sugar sequestration. The efflux of glucose from the liposomes was demonstrated with the addition of boronic acid into the system. Similarly, the influx of these sugars into the liposomes was also shown.

The lipid bilayers of 1,2-dipalmitoyl-sn-glycero-3- phosphocholine (DPPC) have been confined in the pores of silica particles by Schlipf et. al[53]. In this investigation, the lipid mobilities across all the positions (at the core, mid-core and the surface) of the micron-sized nanoporous particles are similar. This indicated the possibility of incorporation of small lipophilic molecules mimicking biological membrane separations in lipid-filled nanopores. Zhou et al. [32] synthesized nanoporous silica thin film membranes with accessible pores on a macroporous anodized aluminium oxide (AAO) support. DPPC lipid bilayers were incorporated into 9 nm silica pores using solvent evaporation and rehydration, in the absence and presence of 4-(N-Boc-aminometyl) phenylboronic acid (BA) embedded in the bilayers. This system, used to test the ability of separation of saccharides such as glucose, xylose and cellobiose, was found to be a promote the flux of saccharides. In the absence of boronic acid, lipid filled pores provide a better barrier to small hydrophilic molecules than lipid bilayers that span the surface of the silica nanopores. However, to the best of our knowledge, there has been no study which examines the effect of increasing concentration of solute molecules on the structure of lipid bilayers in nanoconfinement. This knowledge would be important to designing nanoconfined lipid bilayers with embedded biomimetic carrier molecules.

In this work, we quantify the effect of phenyl boronic acid incorporation in DPPC bilayers on their gel to fluid phase transition, as measured using Differential Scanning Calorimetry (DSC). This phase transition in lipid filled micron-sized silica particles, with nanopores of mean diameter 7.4 nm and 11.7 nm, are compared to free liposomes. Changes in the phase transition temperature were used to determine the partition coefficient of phenylboronic acid in both liposomes and nanoconfined lipid systems.

## 2.2 Experimental Section

### 2.2.1 Materials

Polyethylene oxide (PEO)- polypropylene oxide (PPO)-PEO triblock copolymer (P123, average Mn ~5,800), cetyltrimethylammonium bromide (CTAB, ≥99%) potassium phosphate buffer tablets, chloroform (≥99%) were purchased from Sigma Aldrich; Ethanol (anhydrous) was purchased from VWR; 4-(N-Bocaminometyl) phenylboronic acid (BA, 97%) was purchased from Frontier Scientific.; 1,2-dipalmitoyl-sn-glycero-3- phosphocholine (DPPC, >99%) was purchased from Avanti Lipid; polycarbonate membrane filters of pore size 0.2μm (200 nm) and diameter 25mm were purchased from GE Healthcare-Whatman

### 2.2.2 Synthesis of spherical mesoporous silica particles

Spherical mesoporous silica particles SBAS (Santa Barbara Amorphous Silica) were prepared using the procedure of Schlipf et al. [53] Initially, 0.465 g of CTAB was dissolved in 20 mL of deionized water. The mixture was then added to 3.10 g P123. This solution was placed at room temperature and stirred vigorously while 7.8 mL of 200 proof ethanol and 45.9 mL of 1.5 M HCl were added to it. After the P123 was seen to be completely dissolved, 10 mL of TEOS was slowly added drop by drop. The solution mixing was carried out for 2 hours. At the end of 2 hour period, the solution was poured into a Parr 4748 Teflon lined vessel- which had been kept prior to its usage

at the hydrothermal aging temperature between 60°C and 120°C. The solution was kept at the desired temperature in an oven for 3 days. After a 3 day period, the solution was removed from the vessel and mixed at a high speed till a homogeneous solution was obtained. After homogenization, it was filtered and rinsed with deionized water. After filtration, the sample was placed into a single walled Whatman cellulose extraction thimble, with the surfactants removed using Soxhlet extraction with 200 mL of 200 proof ethanol over 24 h. The pore diameter (5 – 12 nm) increases with an increase in the hydrothermal aging temperature (60°C -120°C). This is confirmed using measurements by nitrogen adsorption.

## 2.2.3 Materials Characterization using BET

Pore diameter and surface area were measured from nitrogen adsorption measurements (Micromeritics Tristar 3000) conducted at -196 °C. Samples were degassed at 120 °C for a minimum of 4 hours under flowing nitrogen gas before analysis. Specific surface area was estimated using the Brunauer, Emmett, and Teller (BET) isotherm and the pore diameter was estimated as the peak in the pore size distribution calculated by the method of Barrett, Joyner, and Halenda (BJH) using the adsorption curve of the nitrogen adsorption—desorption isotherm.

## 2.2.4 Materials characterization using Scanning Electron Microscopy (SEM)

SEM instrument (Hitachi S-4300) was used to characterize the surface morphology of mesoporous silica nanoparticles. The silica particles were placed on a carbon tape. The particles on the tape were dispersed using a duster spray. The silica particles were sputter coated in a gold palladium alloy prior to carrying out the imaging.

### 2.2.5 Fourier transform infrared spectroscopy (FTIR)

To confirm the presence of silica along with the removal of surfactants such as P123 and CTAB, the particles were characterized using a ThermoNicolet Nexus 470 spectrometer equipped with a narrowband liquid nitrogen cooled mercury cadmium telluride (MCT) detector. Potassium bromide was mixed with around 1.0 percent by weight of silica particles using a pestle and mortar. The pellet was pressed and the spectrum was taken. Each spectrum was collected at a resolution of 4 cm<sup>-1</sup> and 250 scans with IR beam incident perpendicularly through the film.

## 2.2.6 Preparation of liposomes containing boronic acid

To make a mixture of DPPC/BA, 5mg DPPC and 4-(N-Boc-aminometyl) phenylboronic acid (BA), with BA weight percentages varying from 0% to 7% wrt DPPC, were dissolved in 1 mL CHCl<sub>3</sub> and sonicated for 5 minutes. The above mixture was then blow-dried with nitrogen and was further dried overnight. To form bilayers, the dried lipid was rehydrated in 1 mL PBS solution above the DPPC phase transition temperature and sonicated at 47°C for 1 hr. The sample was then sonicated for another 15 minutes while cooling to 30°C. 1 mL of the above solution was then extruded through a polycarbonate membrane, of pore size of 200 nm, a total of 21 times till a clear solution of DPPC liposomes was obtained.

# 2.2.7 Boronic acid (BA) immobilized lipid filled silica particle preparation through evaporation deposition

To make a mixture of DPPC/BA, 20mg DPPC and 4-(N-Boc-aminometyl) phenylboronic acid (BA), with BA weight percentages varying from 0% to 7% wrt DPPC, were dissolved with 1 mL CHCl<sub>3</sub> in a plastic vial and sonicated for 5 minutes. 10 mg silica particles were then immersed in the chloroform solution and sonicated for 25 minutes. The above mixture was then blow-dried with nitrogen and was further

dried overnight. To form bilayers, the dried lipid inside the silica particles was rehydrated in 1 mL PBS solution above the DPPC phase transition temperature and sonicated at 47°C for 1 hour. The sample was sonicated for another 15 minutes while cooling to 30°C. The excess lipid was removed by washing the silica particles with PBS thrice.

### 2.2.8 Confocal microscopy

To label the lipid and boronic acid, 1mL of boronic acid immobilized lipid bilayer filled particles were mixed with 1mL of 1 mM Alizarin red S (ARS) on a shaker for 30 min. The samples were then washed with PBS three times and imaged within 2 hours of preparation using a Leica TSP SP5 confocal microscope. Experiments were performed using a 63x/1.4 oil immersion objective. ARS-BA complex was excited at 514 nm for imaging and emission was collected between 580 nm and 620 nm.

### 2.2.9 Differential Scanning Calorimetry (DSC)

DSC was used to confirm the formation of lipid bilayers within silica particles by measuring the gel to fluid phase transition temperature of pore confined DPPC bilayers. Following the preparation of lipid bilayers within particles, particle suspensions were centrifuged at 1,000\*g to form a small pellet. The pellet was transferred into a DSC sample pan. Thermograms were run on a TA Instruments MC DSC between 25°C and 55°C at a ramp rate of 1°C/min and returned to 25°C at a cooling rate of 1°C/min. The heating cycle was repeated once again from 25°C to 55°C at the same ramp rate. The determination of all the thermoanalytical properties was done using the Universal Analysis software.

### 2.2.10 Calculation of solute partition coefficient

The apparent partition coefficient of the phenylboronic acid between the bulk aqueous phase and the DPPC membrane bilayer,  $K_{m/w}$  was calculated as shown in the equation[129] given below:

$$-\Delta T_m = \frac{R*T_m^2}{\Delta H_{DPPC}} * \frac{K_{m/w}}{55.5 + C_{DPPC}*K_{m/w}} C_S \qquad \text{(Equation 2.1)}$$

where  $\Delta T_m$  is the change in melting temperature with the addition of phenylboronic acid compared to the pure DPPC lipid bilayers,  $T_m$  is the melting temperature of pure DPPC (315 K),  $\Delta H_{DPPC}$  is the phase transition enthalpy (31.4 kJ/mol)[130], R is the gas constant, K  $_{m/w}$ , the membrane-water partitioning,  $C_{DPPC}$  is the lipid concentration and  $C_s$  is the concentration of the boronic acid in the bulk solution. The equation assumes that the depression in  $T_m$  (or  $\Delta T_m$ ) being in proportion to the amount of phenylboronic acid in the bulk solution. The membrane partition coefficient is determined from the equation using a linear regression of  $\Delta T_m$  versus boronic acid concentration in the bulk solution,  $C_s$ , using Equation 2.2

$$K_{m/w} = \frac{55.5*M}{\frac{R*T_m^2}{\Delta H_{DPPC}} - C_{DPPC}*M}$$
 (Equation 2.2)

Linear regression was carried out between  $\Delta T_m$  and  $C_s$  to determine the mean value of slope M. The error in the slope accounts for the upper and lower bounds of the 95% confidence interval for the slope. The values for  $K_{m/w}$  and  $log_{10}(K_{m/w})$ (See Table 6) were determined by error propagation using the upper and lower bounds of the 95% confidence interval determined by linear regression.

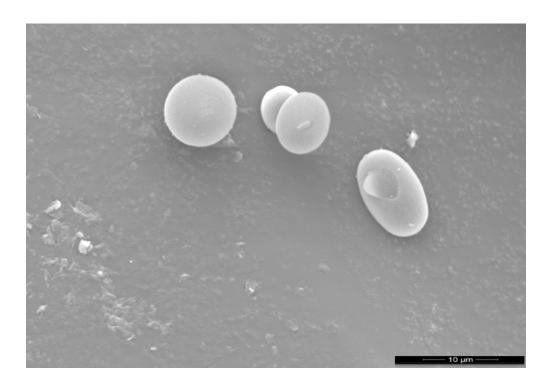
### 2.3 Results and discussion

### 2.3.1 Characterization of SBAS micron-sized silica

The diameters of the ordered pores formed of the SBAS particles can be modified using the hydrothermal aging temperature. Pores are templated from P123 and cetyltrimethylammonium bromide (CTAB) in the aqueous synthesis sol, where the hydrophobic cores of the pore templates expand with increasing aging temperature, creating larger pore diameters [131]. In this study, hydrothermal aging temperatures of 90 °C and 110°C resulted in mean pore diameters of 7.4 and 11.7 nm, as determined by the Barrett- Joyner-Halenda (BJH) method. The scanning electron microscopy (SEM) indicated the formation of near spherical particles that are on the order of 10 microns in diameter. (See Figure 7). The table below (Table 2) provides the surface area and the pore size distribution of the synthesized particles. The nitrogen adsorption isotherm (see Figure 8) indicates that the adsorption of nitrogen onto the pore capillaries follows a Type IV isotherm. This is evident from the fact that the initially, at lower relative pressure regions in the graph, we observe a relatively linear plot which corresponds to the adsorption of monolayers to multilayers of nitrogen. Eventually, pore condensation takes place at higher pressures. Also, one of the main features of such an isotherm is the presence of a plateau close to saturation pressure Po of the bulk liquid[132]. Such a trend in adsorption is usually observed for several class of materials, which include mesoporous materials having pore diameters in between 2-50 nm [133].

FTIR was performed on the SBAS nanoparticles to verify whether the Sohxlet extraction resulted in the removal of surfactants P123 and CTAB. As can be seen in the **Figure 9**, the peak around 3500 cm<sup>-1</sup> indicates the presence of intense broad O-H stretching vibration [134] This maybe the result of water which is hydrogen bonded to

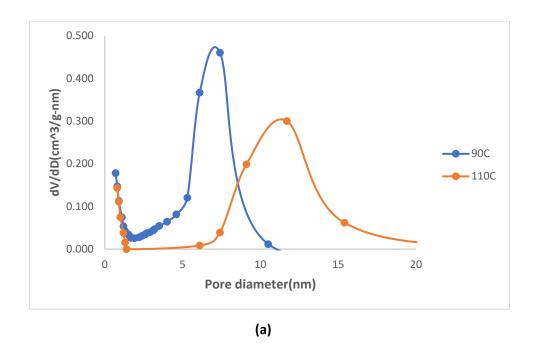
the surface Si-OH groups of the silica matrix. The broad peak observed in between 1000 cm<sup>-1</sup> and 1200 cm<sup>-1</sup> is indicative of an asymmetric Si-O-Si stretching[135]. The sharp peaks for -CH<sub>2</sub> vibrations, which are generally observed between 2800cm<sup>-1</sup> and 3000 cm<sup>-1</sup>[134], are absent. This indicates the success of the Sohxlet extraction process for the removal of the organic surfactant template.



**Figure 7**:Scanning electron microscopy (SEM) image of SBAS micron-sized silica of mean pore size 7.4 nm, synthesized at 90 °C.

Table 2:Surface area and pore size distribution of SBAS micron-sized silica

Sample	Synthesis	Surface Area	Pore Diameter
	Temperature (°C)	$(m^2/g)$	(nm)
SBAS-90	90	789	7.4±1.5
SBAS-110	110	509.8	11.7±2.5



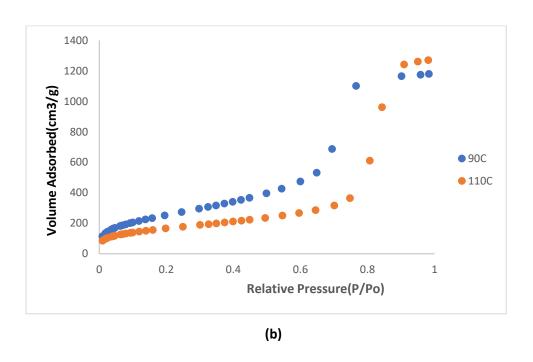


**Figure 8:** (a) Pore size distribution of SBAS micron sized particles prepared at 90°C and 110 °C; (b) Adsorption isotherm of SBAS micron-sized particles

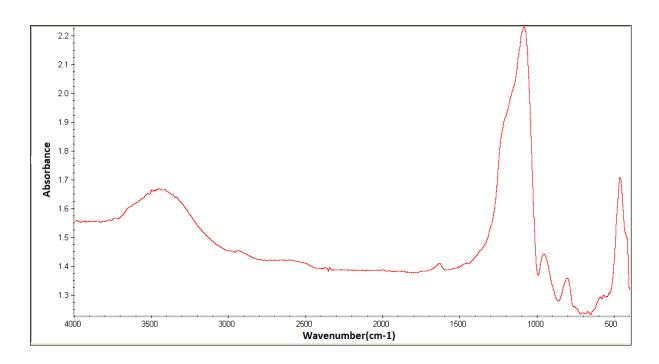


**Figure 9:** FTIR spectra of SBAS micron-sized silica particles mean pore size 7.4 nm, synthesized at 90 °C.

### 2.3.2 Characterization of lipid filled particles

The estimation of the maximum amount of DPPC lipid bilayers which could be localized within the silica nanopores was carried out with the help of the knowledge of partial molar volumes of DPPC bilayers. In an experiment conducted by Miyoshiet al.[136] on the determination of molar volumes of DPPC mixed with cholesterol at various weight fractions, it was found out that the specific volume of DPPC at a temperature of 45°C (above the phase transition temperature of DPPC) was close to 1.025g/cm<sup>3</sup>. The pore volume of the synthesized SBAS particles, which were close to 1.84 cm<sup>3</sup>/g and 1.97 cm<sup>3</sup>/g for micron-sized particles prepared at 90 °C and 110 °C, respectively and determined using BET technique, was used in conjunction to determine the maximum theoretical amount of DPPC which resulted in 20 mg of DPPC per 10 mg of SBAS micron-sized silica.

In order to check the filling of the boronic acid incorporated lipid bilayers of DPPC within the silica nanopores, confocal laser scanning microscopy was employed. This technique enables the imaging of lipids within the porous supports[53]. Confocal microscopy enables excitation of one point in the sample and the fluorescence emission from those points lying out of focus of the laser is blocked by a pinhole before the detector captures it. Subsequently, the whole surface, at a depth of interest, is scanned to give us a two-dimensional construct of the fluorescent molecules within the particles[137]. Typically, the thickness of the DPPC lipid bilayer is around 3-5 nm[138]. The fact that the bilayer thickness is less than the mean pore diameters indicated by nitrogen adsorption measurements suggests that the method of evaporation deposition could result in assembling of lipid bilayers within the pores. The Alizarin Red S(ARS) forms a complex with the boronic acid, which can be called an ARS-BA complex. Figure 10 below shows the fluorescence emission of the ARS-BA complex at a certain depth below the surface of the particle. This could suggest the success of the confinement of DPPC lipid bilayers within the pores of the SBAS particles via evaporation deposition. This observation is also corroborated by the works done by Schlipf et. al[53] and Zhou et al. [32], in which they carry out confocal microscopy to ascertain the confinement of lipid bilayers of DPPC within silica nanopores having sizes greater than the thickness of the lipid bilayers.

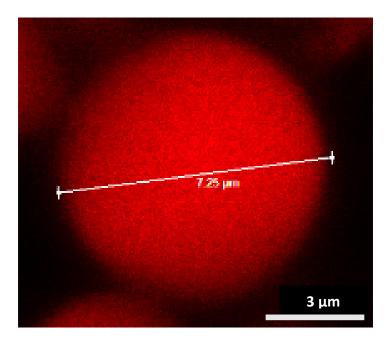


**Figure 10:**Confocal microscopy image of boronic acid incorporated lipid filled silica nanoparticles. The red colour is due to the ARS-BA complex formation. The SBAS micron-sized silica particles have a mean pore size 7.4 nm and synthesized at 90 °C. BA (1% by weight of DPPC) was incorporated in 20mg of DPPC along with 10 mg of SBAS micron-sized silica and ARS was used.

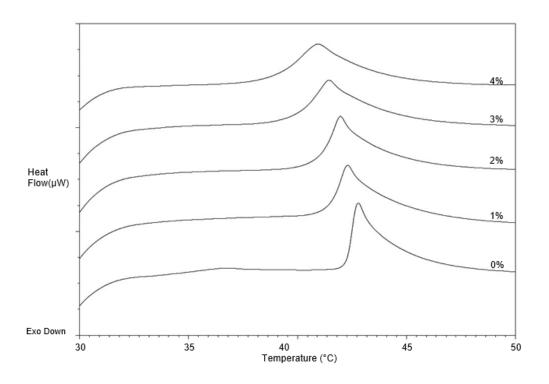
The gel to fluid phase transition and pre-transition temperatures of DPPC lipid bilayers were measured as a function of the addition of boronic acid (from 0-7 weight %) in lipid pore filled silica nanoparticles and liposomes. The pure DPPC melting temperature or main phase transition temperature (T<sub>m</sub>) in liposomal systems is characterized by an endothermic peak at 42.79°C (**Figure 11(a)**). The corresponding onset (T<sub>o</sub>) and full width at half maximum (FWHM) are recorded at 42.23 °C and 1.37°C, respectively. The pure DPPC pretransition exists in the temperature range of 36.47 °C (**Table 3**). The measurements are in close agreement with published values for DPPC liposomes [59]. The main phase transition is the process by which the gel-

phase or the ordered phase of the lipid, having less mobility, is transformed into a disordered fluid phase possessing higher mobility compared to the gel phase[66] [67]. The onset temperature, in the case of lipids, is the intersection of the tangent drawn from the baseline of the DSC curve and the leading edge of the endothermic portion of the DSC curve. The FWHM is the width of the phase transition peak at half the height between the baseline of the DSC curve and the point at which the peak of the phase transition occurs[139].

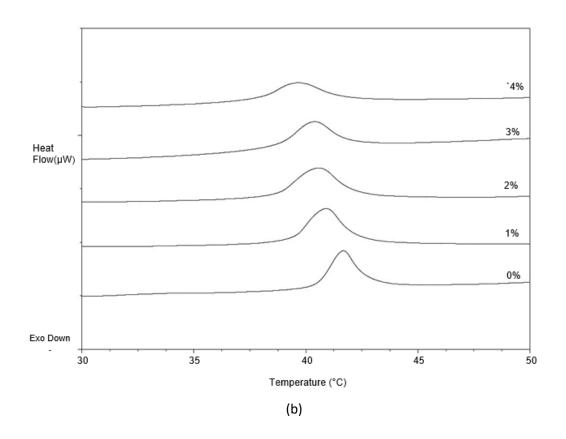
The pure DPPC melting temperature or main phase transition temperature (T<sub>m</sub>) in pore confined systems, synthesized at 90°C and 110°C, is characterized by an endothermic peak at 41.67°C and 41.51°C respectively. **Figure 11 (b) and (c)**). The presence of this transition indicates that confined lipid bilayers exist in the nanoparticles. The corresponding onset (T<sub>o</sub>) temperatures are recorded as 40.44°C and 40.56°C, respectively, and FWHM at 1.54°C and 1.57°C. The pretransition for this system exists in the temperatures of 33.2°C and 32.5°C respectively. (**Table 4 and 5**). The reduction of the main and pre-transition temperatures of confined DPPC relative to DPPC liposomes indicates that confinement affects the structure of lipid bilayers within the nanopores of the micron-sized silica.

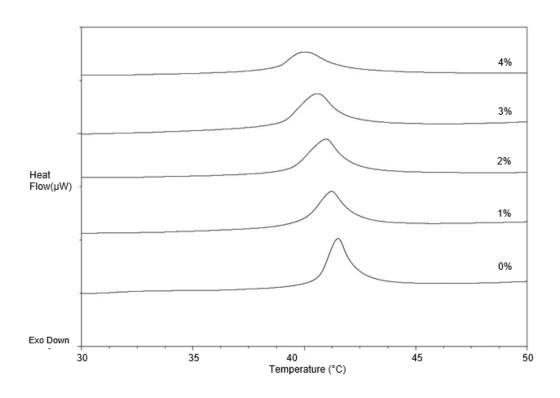
The effects of confinement on lipid bilayers can be compared to confinement effects of non-ionic surfactants, whose structures closely resemble to that of lipids, within nanopores of silica. Müter, Dirk, et al.[140] investigated the effects of confinement of surfactant C<sub>12</sub>E<sub>5</sub> within the nanopores of SBA-15 silica particles, having a mean pore diameter around 8.1 nm, at various filling factors of the surfactant with respect to the maximum amount that can be loaded into the nanopores. It was found that a filling factor closer to maximum loading resulted in the formation of interconnected bilayer patches. However, the thickness of the surfactant layer found at

the pores was much lesser than that on flat surface, indicating a highly distorted or fragmented structure of the bilayer. A similar process of lipid bilayer formation within silica nanopores could be taking place, leading to distortion in the formation of the bilayers. Since the main phase transition temperature is dependent on the extent of cohesiveness of the acyl chains, a reduction in the main phase transition temperature upon confinement is quite likely a consequence of the disruption of the acyl chains.



(a)





(c)

**Figure 11:** DSC thermograms of: (a) DPPC liposomes with boronic acid incorporated from 0 weight percent to 4 weight percent; (b) DPPC bilayers confined within the pores of micron-sized silica (7.4 nm pore diameter) with the incorporation of boronic acid within the bilayers 0 weight percent to 4 weight percent; (c) DPPC bilayers confined within the pores of micron-sized silica (11.7 nm pore diameter), with the incorporation of boronic acid within the bilayers from 0 weight percent to 4 weight percent

**Table 3**:A summary of various parameters obtained of the DSC thermograms for: (a) DPPC liposomes

Concentration	Concentration	Pre-	Onset	Main	Full width at Half
of BA (wt %) in	of BA in bulk	transition	Temperature	Transition	Maximum (FWHM)
DPPC	solution (mol/L)	temperature	(°C)	Temperature	(°C)
	(*10-3)	(°C)		(°C)	
0	0	36.47	42.25	42.79	1.39
1	0.21	34.95	41.43	42.29	1.79
2	0.43		41.00	41.98	1.82
3	0.65		39.95	41.45	2.33
4	0.88		38.97	40.94	2.71
5	1.10		38.02	40.37	2.77
6	1.59		37.46	39.96	3.37
7	1.83		36.80	39.32	3.46

**Table 4**:A summary of various parameters obtained of the DSC thermograms for BA incorporated DPPC bilayers confined in SBAS micron-sized silica nanoparticles of mean pore size of 7.4 nm

Concentration	Concentration	Pre-	Onset	Main	Full width at Half
of BA (wt %) in	of BA in bulk	transition	Temperature	Transition	Maximum (FWHM)
DPPC	solution (mol/L)	temperature	(°C)	Temperature	(°C)
	(da 0, 2)	•		(°C)	
	(*10-3)	(°C)			
0	0	33.45	40.47	41.13	1.37
1	0.85		39.36	40.90	1.75
2	1.72		38.69	40.58	1.91
3	2.61		38.74	40.37	2.12
4	3.51		37.89	39.65	2.38
5	4.44		36.84	39.20	2.55
6	5.39		36.70	39.00	2.83
7	6.35		34.90	38.25	4.59

**Table 5:**A summary of various parameters obtained of the DSC thermograms for BA incorporated DPPC bilayers confined in SBAS micron-sized silica nanoparticles of mean pore size of 11.7 nm

Concentration of BA (wt %) in	Concentration of BA in bulk	Pre-transition temperature	Onset Temperature	Main Transition	Full width at Half Maximum (FWHM)
DPPC	solution (mol/L)	•	(°C)	Temperature	(°C)
	(*10-3)	(°C)		(°C)	
0	0	31.19	40.56	41.51	1.12
1	0.85		39.87	41.22	1.48
2	1.72		39.33	40.96	1.67
3	2.61		38.90	40.58	1.84
4	3.51		38.58	40.01	2.01
5	4.44		37.35	39.52	2.56
6	5.39		37.49	39.00	2.15
7	6.35		35.90	38.42	2.77

The overall trend for the liposomal system is a decrease in main phase transition temperatures with an increase in concentration of boronic acid. In general, the decrease in main phase transition temperatures is believed to be caused because of the disruption of acyl chains of DPPC due to the addition of BA, resulting in the reduction in the temperature for the transition from gel to fluid phase[141]. The continuously decreasing trends in both the systems demonstrate that the BA incorporation increases in the lipid bilayer matrix with increasing bulk BA concentration over the concentration range investigated. The effect of BA incorporation on the gel to fluid phase transition of DPPC liposomes is consistent with previous studies. For example, Ojogun et al.[141] studied the partitioning of a series of nicotinic acid esters (nicotinates) between aqueous solution and DPPC liposomes. An increased chain length of the hydrocarbon group of these compounds was found to elicit a more dramatic response with respect to the disruption of the hydrophobic acyl chains of DPPC. The partitioning of highly

hydrophobic compounds, resulting in chain disruption, can be a highly entropically driven process as evidenced by the studies conducted by Avila and Martinez[142] examining the partitioning of benzocaine (BZC) into bilayers of both DPPC and DMPC. In general, it was found that more energy is required to insert BZC in DPPC bilayers compared to DMPC, probably due to two more methylene groups present in hydrophobic chains of DPPC, resulting in higher van der Waals forces between the tails.

The DPPC confined in silica nanoparticles have a lower pre-transition temperature compared to the liposomal systems in the absence of boronic acid. Also, the pre-transition temperature seems to be abolished at lower boronic acid concentration in DPPC confined systems compared to the liposomal systems. This pre-transition temperature involves change in the acyl chain orientation of the lipids from a tilted gel to a rippled one [143]. This translates into a possibility of stronger interactions involved between the head groups of DPPC and BA to effect such a change in orientation. A stronger BA interactions with DPPC head groups in confined systems is thus probable, thereby abolishing pre-transitions at lower BA concentrations [144].

The bilayer cooperativity is defined by changes to the uniform lipid arrangement during the bilayer phase transition and is affected by incorporation of solutes[141]. The values of Full Width at Half Maximum (FWHM) are being used to measure the cooperativity of the phase transitions. In general, a cooperative unit in a lipid bilayer means that all the acyl chains undergo reordering while there is a transition from the gel phase to the fluid phase. There is an increase in the vibrational motion of the molecules as the transition temperature is approached. This is a cooperative action, thereby changing the orientation. The larger the cooperative unit, the narrower the phase transition temperature range[145]. The bilayer cooperativity in pore confined

systems is generally found to be higher compared to the liposomal systems. This is despite a higher disorder in the acyl chains of the confined systems, indicated by lower main phase transition temperatures, compared to the liposomal systems. Therefore, a lower value of the FWHM indicates higher levels of bilayer cooperativity.

**Table 6:**Table determining the results of the linear regression of Equation 2.1. The slope M is calculated using Equation 2.2. In the table, BA in SBAS-90 denotes boronic-acid incorporated DPPC micron-sized silica synthesized at 90°C and having mean pore size of 7.4 nm; BA in SBAS-110 denotes boronic-acid incorporated DPPC micron-sized silica synthesized at  $110^{\circ}$ C and having mean pore size of 11.7 nm.  $K_{m/w}$  denotes the octanol-water partition coefficient.

System	Slope(M)	K <sub>m/w</sub>	Log <sub>10</sub> (K <sub>m/w</sub> )
	(K/molL <sup>-1</sup> )		
BA in DPPC liposomes	2100±100	9400±1100	3.98±0.05
BA in SBAS-90	370±90	1250±530	3.09±0.18
BA in SBAS-110	390±60	1370±350	3.13±0.11

The octanol-water partition coefficient describes the hydrophobicity or the hydrophilicity of a compound, which might have implications ranging from environmental risk assessment to fate of chemicals in the environment[146]. In the current experiment, the logarithmic values of the partition coefficients were determined by the method elaborated in the Section 2.2.10. The logarithms of partition coefficients measured for liposomal systems were  $3.97\pm0.05$ . Since the slopes of the depression of the melting temperature ( $\Delta T_m$ ) as a function of bulk boronic acid (see Figure 12) were

used to calculate the membrane/water partition coefficients, a higher values of slopes correlates to higher values of partition coefficient. A greater depression in melting point also indicates increased ability of disruption of the acyl chains of the lipid by the molecules. The studies conducted by Xiang and Anderson [147] suggest that a lipid can be divided into regions in which the head group is an area of lower density compared to the lipid tails. The insertion of an aromatic foreign molecule, such as indole [147] and tryptophan [148], possessing polar functional group on one end, within the domain of lipid bilayers results in hydrogen bonding moieties with the head group of the lipids. In the case of insertion of phenylboronic acid within liposomes of DPPC, the hydroxyl atoms attached to the boron on one end could participate in hydrogen bonding with the oxygen atoms of the lipid head group. The remaining portion of the molecule consists of a phenyl ring with its other end attached to bulky hydrophobic substituents such as the oxygen atom of the ester attached to three methyl groups. This hydrophobic part of the molecule would have more affinity towards the lipid tails, which would result in their positioning closer to the centre of the bilayer. This could explain the increased melting point depression of liposomes upon addition of boronic acid. Such a possibility of different parts of a molecule partitioning within different regions of the molecule has been shown to take place in some studies. For example, in an experiment conducted by Neunert, G., et al. [149] on the incorporation of a vitamin tocopheryl glucapyranoside within lipid membranes of DPPC, it was found that the DL- $\alpha$ -tocopheryl  $\beta$ -glucoside portion of the molecule was found to lie in the interior of the membrane as per the molecular simulation studies. However, the sugar component of the molecule was found to be project out of the water-lipid interface of the membrane.

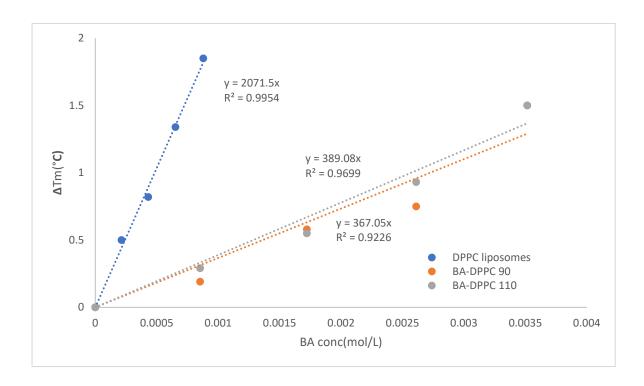


**Figure 12:** Melting point depression of DPPC upon boronic acid addition from 0 weight percentage to 4 weight percentage in : (a) Liposomal systems (blue); (b) boronic-acid incorporated DPPC micron-sized silica synthesized at 90 °C (BA-DPPC 90); (c) boronic-acid incorporated DPPC micron-sized silica synthesized at 110°C (BA-DPPC 110)

On the other hand, the logarithmic values of the octanol-water partition coefficients BA-incorporated lipid pore filled silica nanoparticles, synthesized at 90°C and 110 °C, are 3.09±0.18 and 3.13±0.11, respectively. This shows that the difference in pore sizes of the particles do not result in any observable differences in the partition coefficient of boronic acid within DPPC bilayers. However, compared to the liposomal systems, we find a reduction, of the logarithmic values of the octanol-water partition coefficients, by close to an order of magnitude. The decreases in the melting point

reduction with increasing boronic acid content within lipid bilayers confined in silica nanoparticles compared to liposomal systems could be possibly explained with the help of research conducted on the changes occurring in the lipid head group-water interface upon interaction with the silica nanoparticles. Studies conducted by Guzmán, E., et al.[150] assessed the effects of adsorption of silica nanoparticles on the phase behavior of the monolayers of DPPC mixed with various compounds such as cholesterol [151], palmitic acid [152], and DOPC [153]. These studies revealed that the dispersion of hydrophilic silica nanoparticles within the monolayer matrix results in the disruption of the interfacial structure of the monolayers and the formation of partially hydrophobic nanoparticle-DPPC complexes. This is generally attributed to the electrostatic interactions between the positively charged choline group of DPPC and the negatively charged dissociated silanol groups of the silica nanoparticles[150]. In another study conducted by Chunbo, Yuan, et al.[154] in which the interactions between DPPC liposomes and the silica nanoparticles was studied. It was also inferred via this study that the electrostatic interaction between the positively charged choline groups and the negatively charged silanol groups leads to the disruption of the DPPC liposomes. The presence of hydrophobic complexes at the interface may result in boronic acid partitioning closer to the interface than in the region occupied by the acyl chains.

### 2.4 Conclusion

In this work, we incorporated 4-(N-Boc-aminometyl) phenylboronic acid (BA), at different concentrations, into 1,2-dipalmitoyl-sn-glycero-3- phosphocholine (DPPC) bilayers confined within nanopores of two different mean pore diameters of micron sized silica particles. The higher temperature of synthesis of particles resulted in particles having higher mean pore diameters. The confinement of DPPC into nanopores resulted in the depression in the main phase transition temperatures compared to the

liposomal system. The addition of BA was found to induce disruptions in the acyl chains of the lipid molecules at all concentrations of the solute. The lipid bilayer cooperativity was found to be higher in the confined systems compared to the liposomal systems despite the presence of higher disorder in the hydrophobic acyl chains in the former as suggested by lower main phase transition temperatures. The partition coefficient of BA within the bilayers of DPPC was found to be higher in liposomal systems in comparison to the confined systems. The differences in mean pore sizes of the micron sized silica did not result in any significant differences in the partitioning behaviour of BA within DPPC. The results helped us understand the partitioning of BA in systems in which DPPC was confined into silica nanopores relative to DPPC liposomes. The knowledge of the behaviour of boronic acid in confined systems can help us in designing biomimetic systems, with optimum concentrations of the embedded molecule, to serve the purpose of separation of compounds from dilute aqueous solutions.

## Chapter 3: Effect of lipid pore filling on the colloidal stability of mesoporous silica nanoparticles

### 3.1 Introduction

Mesoporous silica nanoparticles are ideal platforms for surface functionalization due to their high surface area and their tunable pore sizes [155, 156]. This has led to the utilization of mesoporous silica nanoparticles in applications such as drug delivery, biomedical materials[95, 96], and biosensing[97], to name a few. Lipid bilayers coated on the surfaces of silica nanoparticles have been used to improve biocompatibility and biofunction of these systems as nanocarriers[98]. Much research has involved loading of molecules into nanopores, followed by a lipid coating so as to enhance compatibility and possibly uptake of silica nanoparticles by cells in the body[101, 102]. Fluorescent lipid coated nanoparticles can also be used in target specific molecular imaging and cell tracking[103].

Most applications of lipid-coated nanoparticles require their colloidal stability. The presence of silanol groups on the particles results in them having strongly charged surfaces near physiological pH conditions leading to repulsion between them [157, 158]. Zeta potential is the measure of the potential difference between the bulk dispersion medium and a stationary layer called the slipping plane, containing a high concentration of counterions (with a charge opposite to the particle surface) interacting relatively strongly with the surface of the particles[71, 159]. The values of the zeta potential for bare silica nanoparticles is highly dependent on the type of nanoparticles. For particles dispersed in deionized or pure water, reported values vary from -20 mV to -60 mV for various particle sizes [160-162]. Specifically, for a particular method of particle synthesis, such as the Stöber method, the mean particle diameter of 80 nm was found to have a zeta potential of -64 mV[160] and that of 100 nm was found to have a

value of -36 mV[161]. Some of the ways of altering the colloidal stability of bare silica nanoparticles are through the variation ionic strength[163, 164] and the pH[165-167] of the medium. An increase in ionic strength, which is a measure of the concentration[168, 169] and magnitude of charge [170, 171] of electrically charged species in solution, reduces the Debye length or the thickness of the layer of counterions surrounding the charged particle[172]. A higher ionic strength results in better charge screening of the surface of the particles by the counterions which results in quicker drop in the surface potential as a function of the distance from the surface of the particle[173]. Therefore, a higher ionic strength tends to cause aggregation of silica nanoparticles and lower magnitudes of zeta potential. At a pH higher than the isoelectric point of silica (> pH 2.0) [11], on the other hand, results in higher dissociation or deprotonation of the silanol groups on the silica surfaces [83], thereby resulting in more negative zeta potential and better colloidal stability [174].

The effect of coating a lipid bilayer on the surface of silica nanoparticles has also been investigated. These studies have examined the effects of ionic strength, pH and the ratio of amount of lipid to silica nanoparticles on their colloidal stability[86-88]. Moura and Carmona-Ribeiro [86] studied the deposition of zwitterionic phosphatidylcholine (PC) bilayers up silica nanoparticles through vesicle fusion with the surface. It was found that a higher ionic strength of sodium chloride (between 10 mM to 150 mM) promotes an increase in affinity of the PC vesicles for the particles (sizes less than 200 nm), leading to better surface coverage. The resulting zeta potentials of the PC coated lipid bilayers were less in magnitude (around -18 mV) compared to the bare silica nanoparticles (around -45 mV). Moreover, an increase in concentration of the PC vesicles in solution (from 0.01 to 0.7mM), at a constant ionic strength of 150 mM, was found to have a stabilizing effect on the nanoparticles, as evidenced by the

relatively low levels of particle settling observed. The same ionic strength was found to cause sedimentation of the bare silica nanoparticles. An increase in pH of the medium was found to reduce the bilayer deposition. This was attributed to the possible reduction of hydrogen bonding between the phosphate moiety in the PC vesicles and the hydroxyl groups on the silica surface due to a greater number of dissociated silanol groups at higher pH. Moreover, a higher concentration of lipid vesicles coupled with high ionic strength in solution resulted in higher levels of colloidal stability. In another study conducted by the same authors[87] involving deposition of the cationic lipids dioctadecyldimethylammonium bromide (DODAB) and N-[1-(2,3dioleoyloxy)propyl]-N,N,N-trimethylammonium chloride (DOTAP) surfaces, it was found that mixing lipid films (films formed on glass surfaces after evaporating chloroform), instead of already formed lipid bilayers, with silica particles in solutions of low ionic strength (around 1mM of potassium chloride) resulted in causing favourable interactions between the lipids and the hydrophilic silica surfaces due to the lower levels of lipid bilayer digitation in the former method of bilayer deposition on the nanoparticle surfaces. Moreover, the electrostatic interaction between the cationic lipid and the negatively charged silica nanoparticle led to the adsorption of the cationic lipids on silica[88]. Also, in this experiment, it was also found that higher concentrations of the cationic lipids resulted in better colloidal stability, as evidenced by minimum sedimentation of lipid coated particles. The stabilization of lipid enveloped silica nanoparticles is a possible consequence of the presence of hydration forces which are more dominant than the electrostatic repulsive forces at particle separations within 20 Angstroms. It is found to be a very significant force especially for two zwitterionic lipid bilayers coming close together [89]

The process of lipid coating on silica nanoparticles by vesicle fusion involves adsorption, followed by deformation and rupture of the vesicles [48, 99, 175]. Though such lipid-coated nanoparticles demonstrate some degree of robustness and stability, when used for the loading and release of small molecules, potential unwanted interactions of these cargo molecules may arise if embedded within the bilayer matrix, or through interactions with the solid substrate on which the bilayers are supported. This may cause hindrance in the intended function of the incorporated molecule. For example, the interactions of the proteins with the substrate is known to make them immobile and thereby hinder their functioning[175]. Additionally, the existence of pin hole defects has been confirmed using Atomic Force Microscopy (AFM), in the process of deposition of vesicles on hydrophilic solid supports [176].

Assemblies of the zwitterionic lipid dipalmitoylphosphatidylcholine (DPPC) have been confined in the pores of silica nanoparticles by Schlipf et. al[53], who reported that the lipid mobilities across all the positions (at the core, mid-core and the surface) of micron-sized silica nanoparticles having pore sizes close to 9 nm (greater than the thickness of the lipid bilayer) is similar. This indicated the possibility of incorporation of small lipophilic molecules into the lipid bilayers of nanoconfined pores to mimic biological membrane separations. Zhou et al.[32] carried out experiments demonstrating the filling of 10 nm pores of silica membranes, deposited upon porous supports of anodized aluminium oxide(AAO) pores, with DPPC along with the incorporation of a phenylboronic acid derivative within the bilayer matrix. This system, used to test the ability to separate saccharides such as glucose, xylose and cellobiose, was found to be a better barrier to diffusion of small hydrophilic solutes compared to the lipid coated membranes. However, to the best of our knowledge, there has been no

study which tells us about how the inclusion of confined lipid assemblies affects the colloidal stability of submicron mesoporous silica nanoparticles.

In this work, we investigate the effect of the ratio of DPPC lipid to silica nanoparticles on the colloidal stability of lipid-filled nanoparticles of mean size less than 200 nm, where the lipid bilayers are deposited into pores of mean pore diameter close to 8 nm, by the method of evaporation deposition. We compare the changes in the zeta potentials of the lipid filled particles in comparison to the bare silica nanoparticles. We aim to investigate whether the pore filling of lipids within particles has a similar effect in achieving colloidal stability as evidenced from lipid enveloping of silica nanoparticles. The zeta potential measurements of the resulting particles will be analysed in a Phosphate Buffer Saline (PBS, pH 7.4) consisting of 137 mM sodium chloride, 2 mM potassium chloride, and 10 mM phosphate buffer. The results of this experiment could aid in the optimization of the amount of lipids which can be incorporated into nanopores for enhancing the colloidal stability of the system. Additionally, such a system could suggest potential applications for the extraction and sensing of highly lipophilic molecules from dilute solutions.

### 3.2 Materials and Methods

### 3.2.1 Materials

Tetrapropyl orthosilicate (TPOS, 95%) and phosphate buffer saline (PBS) tablets were purchased from Sigma-Aldrich. Cetyltrimethylammonium bromide (CTAB, 99.8%) was purchased from MP Biomedicals; 1,3,5-triisopropylbenzene (TIPB, > 95%), triethanol-amine (TEA, > 98%) and from Alfa-Aesar; ultrapure deionized ultra-filtrated (DIUF) water, ethanol (200-proof), 12 N HCl (ACS grade) from Fisher Scientific; 1,2-dipalmitoyl-sn-glycero-3- phosphocholine (DPPC, >99%)

from Avanti lipid; and polycarbonate membrane filters of pore size  $0.2~\mu m$  (200 nm) and diameter 25 mm from GE Healthcare-Whatman

### 3.2.2 Synthesis of spherical mesoporous silica particles

MSNPs were synthesized using a modification of the method described by Yamada et al.[177], where TIPB was used to swell the CTAB micelles, the pore forming agent, during surfactant-templated synthesis. Initially, 0.56 ml of TEA and 3.0 g of CTAB was added to 360 mL of DIUF water. The solution was kept stirring at 80 °C for 2 hours for complete mixing and emulsion formation and 16 mL of TIPB was added under vigorous mixing. After 30 minutes, 4.77 mL of TPOS was added with constant stirring. Then, the stirring of the solution was done vigorously for 12 hours to obtain white solid particles. The particles were then centrifuged repeatedly and washed and the surfactant was removed by acidic ethanol (167 mL of ethanol with 33 mL of 12N hydrochloric acid) washing three times and finally, they were dried at 84 °C overnight.

### 3.2.3 Materials Characterization using BET

Pore diameter and surface area were measured from nitrogen adsorption measurements (Micromeritics Tristar 3000) conducted at -196 °C. Samples were degassed at 120 °C for a period of 4 h under flowing nitrogen gas before analysis. Specific surface area was estimated using the Brunauer, Emmett, and Teller (BET) isotherm and the pore diameter was estimated as the peak in the pore size distribution calculated by the method of Barrett, Joyner, and Halenda (BJH) using the adsorption curve of the nitrogen adsorption—desorption isotherm.

### 3.2.4 Materials characterization using Scanning Electron Microscopy

SEM instrument (Hitachi S-4300) was used to characterize the surface morphology of mesoporous silica nanoparticles. The silica nanoparticles were placed on a carbon tape. The particles on the tape were dispersed using a duster spray. The

silica nanoparticles were sputter coated in a gold palladium alloy prior to carrying out the imaging.

## 3.2.5 Fourier transform infrared spectroscopy (FTIR)

To confirm the presence of silica in the nanoparticles along with the removal of surfactants such as CTAB, the particles were characterized using a ThermoNicolet Nexus 470 spectrometer equipped with a narrowband liquid nitrogen cooled mercury cadmium telluride (MCT) detector. Potassium bromide was mixed with around 1.0 percent by weight of silica nanoparticles using a pestle and mortar. The pellet was pressed and the spectrum was taken. Each spectrum was collected at a resolution of 4 cm<sup>-1</sup> and 250 scans with IR beam incident perpendicularly through the film.

## 3.2.6 Lipid filled silica particle preparation through evaporation deposition

To fill the pores of synthesized silica nanoparticles with DPPC, samples with DPPC to silica nanoparticle mass ratios of 1:1, 2:1 and 3:1 were dissolved in 1 mL of chloroform and sonicated for 25 minutes. The above mixture was then blow-dried with nitrogen and was further dried overnight. To form bilayers, the dried lipid was rehydrated with PBS to form a 1mg/mL solution of DPPC and silica nanoparticles. The sample was sonicated at 47°C for 1 hr. The sample was sonicated for another 15 minutes while cooling to 30°C.

### 3.2.7 DPPC liposome preparation

To make the liposomes, 15 mg of DPPC were dissolved in 1 mL CHCl<sub>3</sub> and sonicated for 5 minutes. The above mixture was then blow-dried with nitrogen and was further dried overnight. To form bilayers, the dried lipid was rehydrated in 3 mL PBS solution above the DPPC phase transition temperature and sonicated at 47°C for 1 hr. The sample was then sonicated for another 15 minutes while cooling to 30°C. 1mL of the above solution was then extruded through a polycarbonate membrane, of pore size

of 200 nm, a total of 21 times until a clear solution of 5 mg/mL of DPPC liposomes was obtained.

## 3.2.8 Preparation of lipid enveloped silica nanoparticles by vesicle fusion.

Lipid enveloping of bare MSNPs was carried out by preparing 1 mL of the liposome solution prepared in Section 3.2.7 and mixing it with 10 mg of silica nanoparticles for a period of 1 hour to facilitate the process of vesicle fusion.

For one case of lipid-filled particles (1:1 mass ratio of DPPC to silica nanoparticles), lipid enveloping was attempted after lipid filling of the pores for comparison to lipid filling alone. 1 mL of 1 mg/mL of 1:1 DPPC to silica nanoparticles, prepared as per the procedure mentioned in Section 3.2.6, was mixed with 0.25 mg/mL of DPPC vesicles(by taking an aliquot of 50 µL of solution of 5 mg/mL of DPPC vesicles, prepared as per the procedure mentioned in Section 3.2.7, and diluting it to 1 mL using PBS). The mixing was carried out for a period of one hour.

## 3.2.9 Analysis of zeta potential

Zeta potentials of the DPPC vesicles and particles with and without DPPC were measured by dynamic light scattering (DLS) using an Anton-Paar Lightsizer 500 instrument. Around 0.1 mg/mL of solution of DPPC and silica nanoparticles(0.125 mg/mL in the case of 1:1 DPPC to silica nanoparticles enveloped with liposomes of DPPC), prepared by appropriate dilution of the original solutions with PBS, of homogeneous particle suspension in PBS buffer was placed in an omega cuvette (inverted  $\Omega$ -shaped capillary tube) for measurement. During placement of solution inside the capillary tube, extreme care was taken to exclude air bubbles.

### 3.3 Results and Discussion

## 3.3.1 Characterization of mesoporous silica nanoparticles (MSNPs)

MSNPs were synthesized with a target average pore diameter close to 7 nm. The size of the pores was greater than the thickness of DPPC lipid bilayer, which is close to 4 nm [59]. In this process, the CTAB surfactant was utilized for the creation of a template for pore formation and TIPB was mixed for the expansion of the micelle pore templates. The purpose of the acid washing step was to remove surfactants. Spherical particles with diameters around 200 nm were obtained after template extraction, as seen in the SEM image presented in Figure 13. Surface characterization (surface area, pore volume and average pore size) was performed using nitrogen adsorption (Figure 14(a) and Table 7). The pore size distribution, as determined by the Barrett- Joyner-Halenda (BJH) method, is found to have a maximum at around 7.4 nm (See Figure 14(a)). Table 7 provides the surface area and the pore size distribution of the synthesized particles. The nitrogen adsorption isotherm (see Figure 14(b)) indicates that the adsorption of nitrogen onto the pore capillaries follows a Type IV isotherm. This is evident from the fact that the initially, at lower relative pressure regions in the graph, we observe a relatively linear plot which corresponds to the adsorption of monolayers to multilayers of nitrogen. Eventually, pore condensation takes place at higher pressures. Also, one of the main features of such an isotherm is the presence of a plateau close to saturation pressure P<sub>0</sub> of the bulk liquid[132]. Such a trend in adsorption is usually observed for mesoporous materials having uniform pore diameters between 2-50 nm in diameter [133].

FTIR was performed on the MSNPs to a to verify whether the acid extraction resulted in the removal of surfactant CTAB. As can be seen in the **Figure 15**, the peak

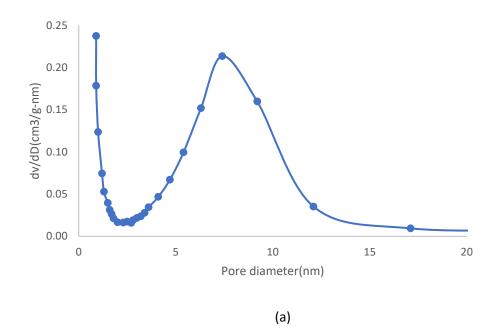
around 3500 cm<sup>-1</sup> indicates the presence of intense broad O-H stretching vibration[134] This includes contributions from water which is hydrogen bonded to Si-OH groups of the silica matrix, in addition to vibrations of Si-OH groups themselves. The broad peak observed in between 1000 cm<sup>-1</sup> and 1200 cm<sup>-1</sup> is indicative of an asymmetric Si-O-Si stretching[135]. The sharp peaks for -CH<sub>2</sub> vibrations, which are generally observed between 2800cm<sup>-1</sup> and 3000 cm<sup>-1</sup>[134], are not distinctly visible. There appears to be a small peak close to 3000 cm<sup>-1</sup>. This could indicate the successful removal of a major portion of the organic surfactant template in the acid extraction.

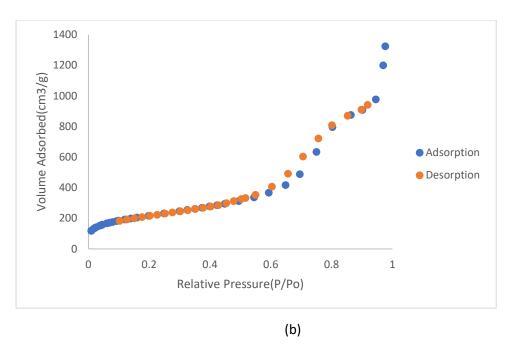
—— 500 nm ——

Figure 13:Scanning electron microscopy (SEM) image of MSNPs

 Table 7:Surface area and pore size distribution of MSNPs

Sample	Pore Volume (cm³/g)	BET Surface Area(m²/g)	Pore Diameter (nm)
Mesoporous silica nanoparticles (MSNPs)	2.07	660.6	7.4±2.3





**Figure 14:**(a) BJH pore size distribution of MSNPs calculated using the adsorption branch of the nitrogen adsorption isotherm; (b) nitrogen adsorption and desorption isotherm of MSNPs. The blue points represent the adsorption isotherm and the orange points represent the desorption isotherm.

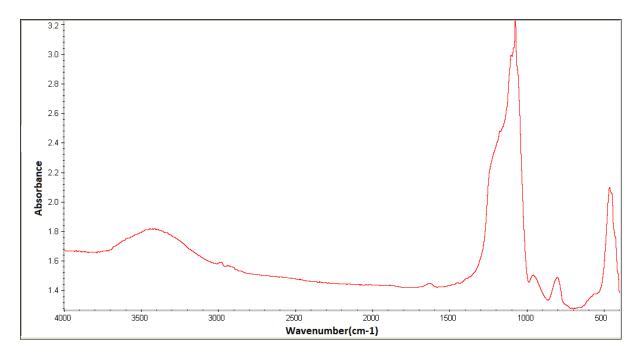


Figure 15:FTIR spectrum of MSNPs in a KBr pellet.

### 3.3.2 Characterization of lipid filled particles

Particles were filled with DPPC using the method of evaporation deposition described in Section 3.2.6. The estimation of the maximum amount of DPPC lipid bilayers which could be localized within the silica nanopores was carried out using the measured pore volume and the partial molar volume of DPPC bilayers. In an experiment conducted by Miyoshiet al.[136] on the determination of density of DPPC mixed with cholesterol at various weight fractions, it was found out that the density of DPPC at a temperature of 45 °C (above the phase transition temperature of DPPC) was close to 1.025 g/cm<sup>3</sup>. The pore volume of the synthesized MSNPs (2.07 cm<sup>3</sup>/g) and this density suggests a maximum theoretical capacity of DPPC of 2:1 by mass, so the baseline loading level was 20 mg of DPPC per 10 mg of MSNPs. It was then desired to assess the effect on the magnitudes of zeta potential of either increasing and decreasing the mass ratio of lipids with respect to MSNPs.

In order to help understand the colloidal stability of lipid filled mesoporous silica nanoparticles, zeta potential ( $\zeta$ ) measurement were taken using dynamic light scattering (DLS). The lipid filled silica nanoparticles, prepared by evaporation deposition, were rehydrated with PBS to form 1 mg/mL of solution of DPPC and silica nanoparticles. Such a concentration was chosen to prevent possible agglomeration of particles during sonication. The  $\zeta$  measurements were conducted using 0.1 mg/mL of the solution which were prepared by taking an aliquot of 0.1 mL of the solution and diluting it to ten times its volume using PBS.

For the bare silica nanoparticles in undiluted PBS media,  $\zeta$  was measured to be -18.6±0.1 mV (See Table 8). The zeta potential of 80 nm silica nanoparticles in PBS, synthesized via Stöber method, has been reported to be -31 mV[14]. In another study,

the zeta potential of 100 nm silica nanoparticles was reported to be -23 mV[178] in PBS. In these two experiments, the method of preparation of the silica nanoparticles was different. These values are different from the zeta potential of silica nanoparticles in media containing only a single electrolyte. For example, the zeta potential was reported to be -45 mV for 120 nm nanoparticles in 0.75 mM NaCl [85]. In another experiment,  $\zeta$  of the same for silica nanoparticles decreased from -62.5 mV to -38 mV when the concentration of NaCl increased from 10 mM to 100 mM [179]. The lower values of zeta potential observed in PBS is due to a high ionic strength of undiluted PBS. This decreases  $\zeta$  by reducing the thickness of the electrical double layer [84].

Lipid enveloping of the bare MSNPs with DPPC was carried out using the same buffer solution by the process described in Section 3.2.8. After enveloping,  $\zeta$  was measured to be -16.4±1.2, which was marginally higher than bare MSNPs. For comparison, Savarala et al. [85] studied the adsorption of 1,2-dimyristoyl-sn-glycero-3-phosphocholine (DMPC) vesicles onto 20-100 nm silica nanobeads and found that  $\zeta$ decreased from around -45 mV to between -20 to -30 mV in 0.05 to 0.75mM NaCl. The amount of DMPC used was enough that complete external surface coverage of the silica nanobeads was ensured. Moura and Carmona-Ribeiro reported that deposition of PC vesicles onto silica nanoparticles at pH 6.3 in DI water reduced  $\zeta$  from -45 mV to -18 mV [86]. In both the cases, the reduction in zeta potential was attributed to the shielding of the negative charge of silica by the zwitterionic DMPC and PC vesicles. In our experiments, the amount of DPPC needed to completely envelope the silica nanoparticles was not determined exactly. However, the estimation of amount of DPPC theoretically required to cover the external surface of MSNPs is  $0.65 \pm 0.01$  nm<sup>2</sup> [180]. Estimating the external surface area of the MSNPs from their radius and pore volume, which is 79 m<sup>2</sup>/g, and considering that the head-group area of DPPC is for per lipid per monolayer in the bilayer, we obtain the theoretical amount of DPPC to cover the surface of MSNPs to be around 0.36 mg per 1.0 mg of MSNPs. In our system, 5 mg of DPPC was mixed with 10 mg of MSNPs to facilitate vesicle fusion, so a small excess of lipid should in principle be available. A small reduction in the zeta potential of MSNPs, upon enveloping with DPPC, could suggest partial coverage of MSNPs by the DPPC vesicles.

In contrast to lipid enveloping, evaporative pore filling of DPPC lipid in the mass ratio of 1:1 with respect to silica nanoparticles results in a sharp decrease in the zeta potential of the nanoparticles to around -9.9 mV. A further increase in the amount of DPPC is shown to further decrease the magnitude of  $\zeta$  close to -5 mV (See Table 8)

Schlipf et al.[53] conducted diffusivity studies on DPPC at the surface and within the pores of micron-sized SBA-15 silica particles. Though the studies were conducted on particles having a range of pore diameters, an important observation made in these studies is the presence of lipid bilayers on the surface of particles having mean pore diameters of around 9 nm, as indicated by the occurrence of diffusivity on the surface of these particles. Lipid bilayers of DPPC are found to have a thickness of around 3-5 nm[138]. The process of evaporation deposition followed by subsequent rehydration results in the assembling of lipids within the pores[53]. The lipid bilayers covering the surface of the silica nanoparticles, in our experiments, could be causing the reduction in the values of zeta potential of lipid filled particles. The presence of unilamellar vesicles on nanoparticles of 100 nm diameter has been confirmed by TEM studies[181]. Anderson et al.[182] conducted studies on the coverage of DMPC vesicles on borosilicate glass substrates, having similar properties as silica surfaces. The  $\zeta$  measurements of the charged glass surface, as a function of ratio of the amount of injected DMPC vesicles to the amount required for full surface coverage, demonstrated

a decrease in magnitude with ratios. It was observed that a ratio greater than 20 was found to cause a drastic reduction in the magnitude of  $\zeta$  from close to -30 mV to -10 mV. This was interpreted to be the ratio required for initiation of rupture of vesicles and subsequent bilayer formation.

Some studies have shown that, despite the reductions in magnitudes of zeta potential observed upon deposition of zwitterionic lipids of PC on the surface of silica nanoparticles, an increase in the concentration of the lipid in solution was found to reduce the sedimentation of the silica nanoparticles[86]. In the case of cationic lipids DODAB and DOTAP, an increase in the concentration of lipids, besides increasing the magnitude of the zeta potential of silica nanoparticles with respect to the bare ones, also resulted in minimal sedimentation of the nanoparticles [87]. The stabilization of lipid enveloped silica nanoparticles is a possible consequence of the presence of hydration forces which are more dominant than the electrostatic repulsive forces at particle separations within 20 Angstroms. It is found to be a very significant force especially for two zwitterionic lipid bilayers coming close together[89]. We attempted to assess the effect on  $\zeta$  of enveloping of DPPC vesicles around silica nanoparticles whose pores were already filled with a 1:1 mass ratio of DPPC. The zeta potential of such particles was found to be -2.4±0.4 mV. These values were very similar to that of DPPC liposomes, which in our experiments was found to be -2.2±0.7 mV in PBS. This is in close agreement to  $\zeta$  reported in the literature for DPPC liposomes in 150 mM NaCl solution, is in the range of 0 to -5 mV[183]. There could be several reasons for the observed reduction in ζ for 1:1 mass ratio lipid-filled MSNPs (-9.9 mV) after coating with DPPC bilayers (-2.4 mV). A general mechanism of enveloping of vesicles onto the surface of silica nanoparticles involves the adsorption of the vesicles, followed by its deformation and eventually, the rupturing of the vesicle [48, 99, 175]. The loosely

adhered vesicles may require additional stress from surrounding vesicles to cause the rupture. The ruptured vesicles may fuse by the influence of the edges of the already present bilayer patches [184]. In our system, there is a possibility that the bilayer patches existing on the surface of silica nanoparticles may rupture and fuse together in the presence of the externally introduced DPPC vesicles. These bilayer patches could be loosely adhered onto the surface of the silica nanoparticles and the rupturing could possibly be taking place in the presence of external DPPC vesicles. Subsequently, the hydrophobic lipid tails lying near bilayer edges could fuse and form a more continuous bilayer[185]. It is also possible that the introduced DPPC vesicle fuses along with the existing bilayer patches on the silica nanoparticles, thereby causing a sharp reduction in the zeta potential. Cryo-Transmission Electron Microscopy (Cryo-TEM) has been used to enable visualisation of the process of deposition of neutral zwitterionic lipid vesicles of 1-palmitoyl-2-oleoylphosphatidylcholine (POPC) and DMPC onto silica surfaces[186]. To be able to better visualise the process of lipid filling of silica nanoparticle, the usage of Cryo-TEM could enable us to assess the process by which the surface coverage of silica nanoparticles takes place by increasing the mass ratio of lipids to silica nanoparticles. Additionally, it could also enable us to visualise how the introduction of liposomes to already filled lipid vesicles influences the surface coverage of silica nanoparticles.

It is imperative to note that the knowledge of the changes in hydrodynamic diameters of the silica nanoparticles, upon increasing deposition of lipids, in conjunction with the changes in the zeta potential of the nanoparticles will enable us to better assess the colloidal stability of the lipid filled silica nanoparticles. Studies conducted on deposition of zwitterionic PC vesicles on silica nanoparticles demonstrated a concomitant decrease in their hydrodynamic diameters [86]. The settling

velocities of nanoparticles is found to be proportional to the hydrodynamic diameters of the nanoparticles[182]. A lower settling velocity would mean lower sedimentation and increased colloidal stability. A visual study of 1 mg/mL of solutions of DPPC+MSNPs in our experiments at all the lipid to MSNPs mass ratios seemed to be colloidally stable over a period of 0.5 hours (data not shown). However, it may be beneficial to assess the colloidal stability of the nanoparticles for extended time periods and visually observe the sedimentation of the MSNPs at different time intervals.

**Table 8:**Zeta potential of various MSNPs. In the above figure, LE MSNPs refers to lipid enveloped MSNPs; LPx MSNPs refer to lipid filled silica nanoparticles, where x equals 1,2,3 refers to lipid to silica nanoparticle mass ratios of 1:1,2:1 and 3:1 respectively;LP1 LE MSNP refers to lipid filled silica nanoparticles with 1:1 mass ratio of lipid to silica nanoparticle with an enveloping of DPPC vesicles. The measurements are taken in PBS solution, containing 137mM of sodium chloride, 2mM of potassium chloride and 10mM of phosphate buffer

Sample	Zeta Potential(mV)
Bare MSNPs	-18.6±0.1
LE MSNPs	-16.4±1.2
LP1 MSNPs	-9.9±1.7
LP2 MSNPs	-5.3±0.7
LP3 MSNPs	-4.3±0.9
LP1 LE MSNP	-2.4±0.4
DPPC liposomes	-2.2±0.7

### 3.4 Conclusions

In this work, the method of evaporation deposition was used to fill the pores of silica nanoparticles with 1,2-dipalmitoyl-sn-glycero-3- phosphocholine (DPPC) and

assess the effect of increasing the mass ratio of lipid to silica nanoparticles on the zeta potential and colloidal stability of the nanoparticles. An increase in the mass ratio resulted in observable reductions in magnitudes of zeta potential of the resulting nanoparticles compared to bare silica nanoparticles. Lipid enveloping of pore filled silica nanoparticles results in zeta potentials comparable to that of DPPC liposomes. The reductions in zeta potentials of the lipid filled silica nanoparticles were hypothesized to be the result of several isolated lipid bilayers covering the exterior surface of the nanoparticles, besides filling the nanopores. The complete assessment of colloidal stability of the system necessitates obtaining of information regarding the changes in hydrodynamic diameters and the settling behaviour, with extended time periods, of the lipid filled particles in conjunction with the obtained values of zeta potential of the system. The possibility of using cryotransmission Electron Microscopy to visualise the formation of bilayers on the external surface of silica nanoparticles in the process of pore of filing was suggested. The determination of the optimal amount of lipids that can be deposited into the silica nanopores would enable the designing of systems involving extraction and sensing of highly lipophilic molecules form dilute solutions.

# Appendix A: Dye uptake studies of Sulforhodamine 101 within amine functionalized radial mesoporous silica nanoparticles.

#### A.1 Introduction

Mesoporous silica nanoparticles have received immense attention over the recent years[90-92]. Their advantages for applications in separation, catalysis, and biomolecule loading are their uniform and tunable pore sizes [93], large surface areas and pore volumes [94]. There have been many reports of release of guest molecules, such as drugs, encapsulated within pores of silica nanoparticles in the presence of external stimuli such as pH[187-190]. The drug molecules, as doxorobucin (DOX), are found to have a release percentage of 20 wt.% DOX within 100 h at a pH 7.4. In acidic environment, about 50 wt.% (pH = 5.0) and 65 wt.% (pH = 3.0) of DOX was released within 100 h, at higher pH and the lowering of the pH has shown to effect their release[191]. The coating of silica nanoparticles with a polymer, such as poly(methacrylic acid-*co*-vinyl triethoxylsilane) (PMV), can act as a molecular switch. Ibuprofen loaded in such systems was found to show a low release(15 wt%) at pH of 4 or 5 and a burst of release at pH close to 7.5[192]. This was attributed to polymer shell opening at high pH compared to lower ones.

To the best of our knowledge, there has been no study involved in determining the pH dependency of encapsulation and release profiles of fluorescent dyes. Sulforhodamine 101 has been used extensively for the purpose of cell labelling[193-195]. Amine functionalized silica nanoparticles, on the other hand, have been used as vehicles of targeted delivery for the treatment of various cancers[196-198]. There have been studies conducted on removal of anionic textile-based dyes by amine functionalized silica nanoparticles[199]. A pH of 2 was found to result in the dye removal of around 80% for an adsorption time of 60 minutes.

In this work, we attempt to load the fluorescent dye of Sulforhodamine 101, in increasing concentrations from 0.1-2.0 mg/mL, into pores of amine functionalized mesoporous silica nanoparticles at pH 2. After determining the maximum loading capacity of the particles, the release percentages of the encapsulated dyes will be compared, at two different pH values of 10 and 12. The results from this study can enable optimization of parameters for sensing and imaging based applications.

### A.2 Experimental section

#### A.2.1 Materials

Tetraethyl orthosilicate (TEOS, 99%) and Sulforhodamine 101(>99%, laser grade acid-free) were obtained from Acros Organics; (3-Aminopropyl)triethoxysilane (APTES, 99%) from Sigma-Aldrich;; cetyltrimethylammonium bromide (CTAB, 99.8%) from MP Biomedicals; Ethanol (200 proof), ultrapure deionized ultra-filtrated (DIUF) water; and 6 N HCl (ACS grade), and 29.3 wt% NH4OH solution from VWR.

### A.2.2 Synthesis of radially oriented mesoporous silica nanoparticles

Samples were prepared on the basis of the procedure of Liu et al.[200] The initial reactants had molar ratios of 1 TEOS:0.3 CTAB:11 NH<sub>3</sub>:58C<sub>2</sub>H<sub>5</sub>OH:144 H<sub>2</sub>O. Particles were formed by mixing all reagents in the reverse order listed. The TEOS was added slowly over 1 min. To be more precise, 7.44 mL of TEOS, 3.64 g of CTAB, 24.4 mL of 29.3 wt% NH<sub>4</sub>OH, 112.7 mL of C<sub>2</sub>H<sub>5</sub>OH and 70.9 mL of water were used. After aging the solutions for 2 h at room temperature, white powder precipitates were filtered and washed with deionized water. Dried samples were twice extracted with acidic ethanol (150 mL ethanol with 3 mL of concentrated aqueous HCl) to remove the surfactant.

# A.2.3 Synthesis of amine functionalized mesoporous silica nanoparticles(MSNPA)

Amine functionalized silica nanoparticles were obtained by condensing (3-aminopropyl) triethoxysilane (APTES) on the particle surface using a modified version of the methods reported in the literature[201, 202]. 200 mg of ordered mesoporous particles were sonicated in 25 mL of dry ethanol for 15 min and a uniformly dispersed solution was obtained. 0.5 mL of APTES was added drop wise under constant stirring and the solution was kept stirring overnight in a closed environment at room temperature. Particles were centrifuged at 17,000 rpm followed by repeated washing with dry ethanol and cured at 84°C overnight. After curing, particles were stirred in excess ethanol for 24 hours to remove any remaining, loosely bound amine groups. The functionalized particles were again washed 3 times with dry ethanol and dried in an oven at 84°C.

## A.2.4 Calibration curve for Sulforhodamine 101 dye uptake and dye release using amine functionalized silica nanoparticles

To prepare a calibration curve at pH 2, a 0.1 mg/mL solution of sulforhodamine 101 was made. 6 N hydrochloric acid solution was used for pH adjustment. From that stock solution, dilutions of 1/100<sup>th</sup>, 1/200<sup>th</sup>, 1/400<sup>th</sup> and 1/800<sup>th</sup> were performed using an acidic solution of pH 2. At pH 10 and 12, a 0.1 g/L solution of sulforhodamine 101 was made. A 29.3 wt% ammonium hydroxide (NH<sub>4</sub>OH) solution was used for adjusting the pH. From that stock solution, dilutions of 1/1000<sup>th</sup>, 1/2000<sup>th</sup>, 1/4000<sup>th</sup> and 1/8000<sup>th</sup> were performed using alkaline solutions of pH 10 and 12. The fluorescence readings were taken in a BioTek (Winooski, VT) plate reader. The excitation and emission maxima wavelength of the dye was found out to be 586 and 610 nm, respectively.

# **A.2.5** Solution depletion studies of Sulforhodamine 101 dye using amine functionalized silica nanoparticles

The amine functionalized silica nanoparticles were soaked in DIUF water overnight. For this study, eight stock solutions of Sulforhodamine 101 dye with concentrations ranging from 0.1-2.0 mg/mL in an acidic solution of pH 2 were prepared. For each dye concentration, triplicates of 1 mL of the dye solution mixed with 5mg of amine-functionalized silica nanoparticles were prepared except for the 1.5 and 2.0 mg/mL concentrations (for which six samples were prepared). Dye solutions with particles were mixed overnight at room temperature. After mixing, the vials containing the sample were centrifuged at 17000 g for five minutes. The supernatant was then analysed to quantify unbound dye particles using the BioTek plate reader. The equilibrium uptake of the dye was calculated as:

$$q(mg/g) = \frac{(C_0 - C_e)}{m} * 1000$$

where q is the equilibrium uptake of the dye (in mg/g);  $C_0$  is the initial dye concentration (in mg/mL);  $C_e$  is the equilibrium dye concentration (in mg/g) and m is the mass of the MSNPA(in mg).

# A.2.6 Sulforhodamine 101 dye release quantification from amine functionalized silica nanoparticles

After adsorbing Sulforhodamine 101 dye from 1.5 and 2.0 mg/mL solutions onto MSNPA, the supernatant was removed and 1 mL of alkaline solutions

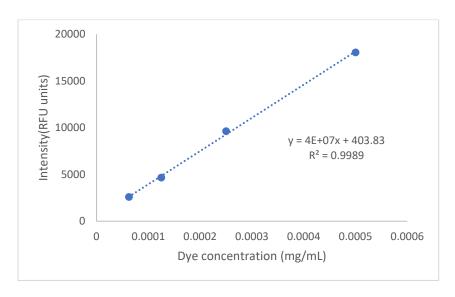
of pH 10 or 12 was added. Release was measured in triplicate samples for each pH. The fluorescence intensity of the released dye, from the MSNPA, was quantified using the BioTek plate reader. The corresponding concentration of the  $dye(E_0)$  was back-calculated using the calibration curves. The equation of the dye release percentage(R) is as follows:

$$R(\%) = \frac{E_0}{C_0 - C_e} * 100$$

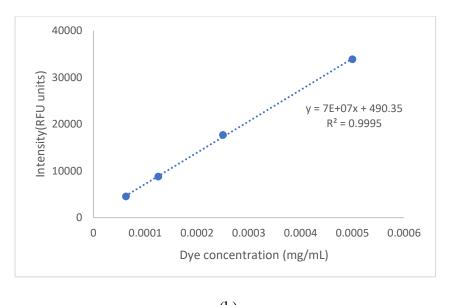
where  $E_0$  is the concentration of the dye released (mg/mL);  $C_0$  is the initial dye concentration(in mg/mL) prior to uptake;  $C_e$  is the equilibrium dye concentration (in mg/mL) after uptake.

#### A.3 Results and Discussions

The calibration curves, plotting the fluorescence intensity of the Sulforhodamine 101 dye versus its concentration in the solution at pH 2,10 and 12 are shown in **Figure 16.** It is observed that the intensity of fluorescence is higher for higher values of pH at the same dye concentrations.



(a)



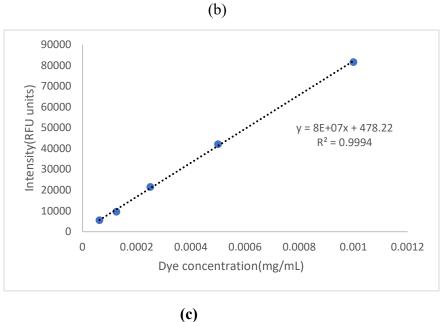


**Figure 16:**Calibration curves of sulforhodamine 101 dye in: (a) pH2; (b) pH 10; (c) pH 12

The dependence of the initial concentration of the dye on its uptake by MSNPA is shown in **Figure 17.** It is observed that the saturation or the maximum uptake of Sulforhodamine 101 by the MSNPA occurs at around 350 mg of the dye per gram of MSNPA. Due to the tendency of the nitrogen atom to be a better electron donor compared to the oxygen atom, an acidic pH possibly leads to the favourable protonation of the amine groups present on the silica surface compared to the negatively charged oxygen atom in Sulforohodamine 101. The negatively charged sulforhodamine 101 group is transferred from the solution to the pores of the silica nanoparticles due to the

presence of electrostatic interaction between the positively charged amine groups and the negatively charged oxygen atom.

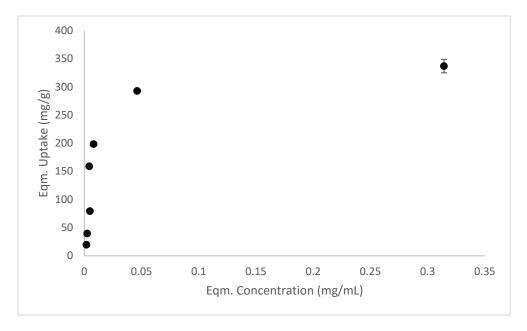


**Figure 17:**Uptake of Sulforhodamine 101 dye by MSNPA as a function of dye remaining in the solution at a pH of 2. Error bars show the standard deviation in the readings of the uptake values taken in triplicates.

The **Table 9** shows the dependence of the initial dye concentration, used for the uptake of the dye at pH 2, and the pH on the release percentages of the dye. In general, a higher percentage is observed at higher values of pH and higher initial dye concentrations used. A higher pH could result in the abstractyion of the proton from the nkitrogen atom by the hydroxyl ions introduced in solution. This results in the elimination of the electrostatic interaction between the atoms. Therefore, the dye release at higher pH could take place.

These results demonstrate the capability of mesoporous silica nanoparticles to capture high amounts of dyes at lower pH and effect a significant release in alkaline environments.

**Table 9:** Release percentages of Sulforhodamine 101 dye from MSNPA at pH 10 and 12 at different initial concentrations of the dye before uptake.

pH	Initial dye	Dye release (%)	
	concentration(mg/mL)		
10	1.5	$48.4 \pm 1.4$	
	2.0	$75.6 \pm 6.7$	
12	1.5	83.1 ±14.9	
	2.0	90.0 ±14.1	

Acknowledgements: I would like to acknowledge the efforts taken by Ms. McKenna Clinch in carrying out the relevant experiments for this project.

# Appendix B: Attachment of acryl-modified DNA onto thiol attached glass coverslips

#### **B.1** Introduction

In the past several years, there have been several research efforts taken to utilise nucleic acids such as DNA for various applications ranging from imaging, diagnostics and sensing[203-206]. In particular, for the successful sensing to take place, it is necessary to develop approaches involving the immobilization of DNA onto surfaces[198, 207]. The attachment of DNA has been carried on several types of surfaces such as gold[208, 209], carbon[210, 211], glass[212-214]etc., to name a few.

The utilisation of ultraviolet(UV) radiation has been a frequently explored method for the attachment or immobilisation of DNA onto surfaces[215-218]. The surfaces are typically modified using an alkene[219, 220] or a thiol[221, 222] moiety, followed by the attachment of the DNA molecules using UV chemistry.

X-ray Photoelectron Spectroscopy (XPS) is a widely used surface sensitive technique for the measurement of elemental compositions of the material surface[223]. The energy of the electrons emitted from the surface, upon incidence of an X-ray, is measured using this technique. This energy is the characteristic of atom of the bombarded element and this helps in its identification[224]. XPS has been widely used to characterize or confirm the attachment of DNA on surfaces[225-228].

In this work, we aim to functionalize the surfaces of circular glass coverslips using (3-mercaptopropyl) trimethoxysilane (MPTMS). Subsequently, the success of the thiol modification of the coverslips and the dependence of the presence of a photoinitiator on the successful covalent linkage of the acryl-modified DNA oligonucleotide, onto thiol modified surfaces, via UV thiolene click chemistry will be analysed using XPS.

## **B.2** Experimental section

#### **B.2.1** Materials

Nochromix powder, ethanol (200 proof), ultrapure deionized ultra-filtrated (DIUF) water, H<sub>2</sub>SO4 (95-98% in water) and 29.3 wt% NH<sub>4</sub>OH solution were purchased from VWR International; (3-mercaptopropyl)trimethoxysilane (MPTMS, 95%) from Alfa Aesar; 50 mm diameter round glass coverslips from Electron

Microscopy Sciences; 2-hydroxy-4'-(2-hydroxyethoxy)-2-methylpropiophenone (≥98.0% by HPLC, water-soluble photoinitiator or WSP) from TCI America; DNA oligomer of 5'-/5Acryd/CGC TCC CAA CCG CCT CAT TAT G-3'(MW=6838.5g/mol) from Integrated DNA Technologies; and mounted UV LED lamp (wavelength: 365 nm; irradiance: 17.6 μW/mm² at a distance of 200 mm from the source) from Thorlabs Inc.

## **B.2.2** Cleaning of glass coverslips

The glass coverslips were cleaned by submerging them in a Norchromix solution (a solution containing Norchromix oxidizer powder in concentrated sulfuric acid) overnight. The glass coverslips were then rinsed with DIUF and dried in an oven.

## **B.2.3** Thiol modification of glass coverslips

The glass coverslips were modified based on the procedure described by Bertin and Sclhaad [229]. A 10  $\mu$ L drop of MPTMS was placed on each of the cleaned glass coverslips and were baked in an oven kept at 150°C for twenty minutes. The coverslips were then washed thoroughly with ethanol to remove excess unattached thiol groups.

#### **B.2.4** DNA attachment to thiol attached glass coverslips

The attachment of DNA oligomer was carried out by slight modification of the procedure provided by Escorihuela et al. [207]. 20  $\mu$ L of 0.38mg/mL of the DNA oligomer in RNAse free water was placed onto the thiol modified coverslips followed by the addition of 20  $\mu$ L of 0.05% of WSP onto the DNA droplets ensuring complete coverage of the top surface of the coverslip. The surface was then illuminated with the UV LED for thirty minutes. After the completion of the reaction, the surface was thoroughly rinsed with RNAse free water. A control sample, without WSP, comprising 20  $\mu$ L of 0.38mg/mL of the DNA in RNAse free and 20  $\mu$ L of RNAse-free water was also illuminated with the UV LED for 30 minutes.

# **B.2.5** Analysis of thiol attachment and DNA attachment using X-ray photoelectron spectroscopy (XPS)

The presence of -SH groups on thiol modified glass slides and the changes in the percentage of carbon on the glass slides during DNA oligomer attachment was measured using a K-Alpha XPS Instrument (Thermo Scientific). Prior to carrying out the analysis, the samples were stuck onto a carbon tape, which was further stuck onto a sample stage. Vacuum was applied to the sample chamber till the pressure reached 5\*10<sup>-8</sup> mbar. High definition elemental scans of carbon, oxygen, silicon and sulphur

were taken for thiol modified glass slides. For DNA oligomer modified conjugated glass slides, high definition scans were taken for carbon, oxygen, silicon, sulphur, nitrogen and phosphorus. The results of the XPS were analysed using the Thermo Scientific<sup>TM</sup> Avantage Software.

### **B.3** Results and Discussion

The addition of MPTMS onto cleaned glass coverslips is expected to result in the formation of thiol groups on the surface of the coverslips. Table B1 below shows us the changes in elemental composition upon addition of MPTMS. Since MPTMS contains carbon atoms due to the presence of propyl groups and thiol moiety attached to the propyl groups, the addition of MPTMS is expected to lead to a concomitant increase in the carbon and sulfur content. Fig. B1(g) shows us the presence of an XPS peak around 164eV. This is found to be a characteristic peak of sulfur atom bonded to carbon as a single bond.

The attachment of DNA oligomer was subsequently carried out using thiolene click chemistry, using ultraviolet (UV) radiation, in the presence and absence of the water-soluble photoinitiator. **Table 10** provides the changes in the elemental compositions of the atoms upon carrying out the reaction. An increase in the carbon content by around 10% in the DNA modified coverslip is observed compared to the thiol modified coverslip. The XPS spectra of both the coverslips are shown in **Figure 18**. It can be observed that the addition of DNA in the presence of the photoinitiator leads to the formation of a nitrogen peak at around 400eV. (**Figure 19(i) and (j)**). The nitrogen peak could be a possible result of the presence of nitrogen atoms in DNA. For all other elements, a significant change in the peaks is not observed. It could be concluded that the increase in the amount of carbon in DNA modified coverslips combined with a noticeable presence of an XPS peak of nitrogen could indicate the necessity of the presence of a photoinitiator to carry out the DNA attachment onto the thiol groups.

On the other hand, the absence of the photoinitiator while carrying out the UV reaction indicates the possibility of unsuccessful DNA attachment as per the elemental compositions shown in **Table 11**. It can be clearly observed that the change in the carbon content upon attempt to attach DNA onto the coverslips is negligible. Moreover, a look at the **Figure 20(i) and (j)** indicates the absence of a nitrogen peak at 400 eV,

suggesting that the absence of a photoinitiator could lead to the non-attachment of DNA onto the coverslips.

**Table 10**:Elemental compositions of clean glass coverslips and thiol modified glass coverslips

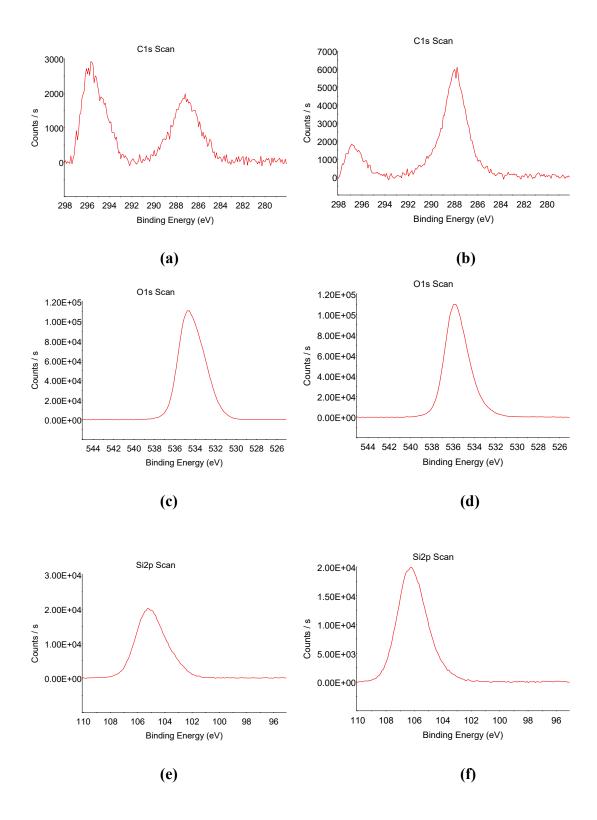
	Carbon (%)	Oxygen (%)	Silicon (%)	Sulfur (%)
Clean glass coverslips	5.17	68.52	26.3	-
Thiol modified glass coverslips	49.32	26.87	15.8	8.01

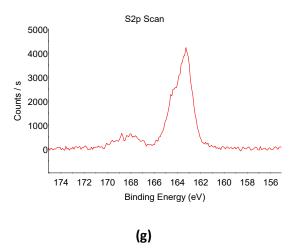
**Table 11**:Elemental compositions of thiol modified coverslips and DNA modified thiol functionalized coverslip using 0.05% by weight of WSP

	Carbon (%)	Oxygen (%)	Silicon (%)	Sulfur (%)
Thiol modified glass coverslips	58.84	23.06	13.07	5.04
DNA modified glass coverslips with WSP	68.28	19.88	7.84	2.95

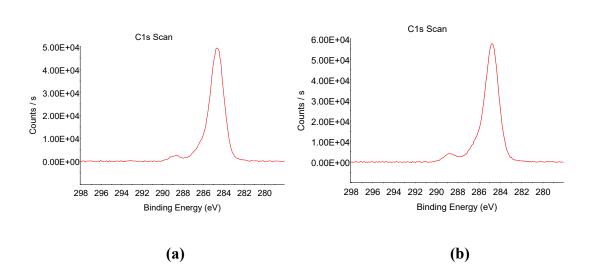
**Table 12**: Elemental compositions of thiol modified coverslips and DNA modified thiol functionalized coverslip without WSP

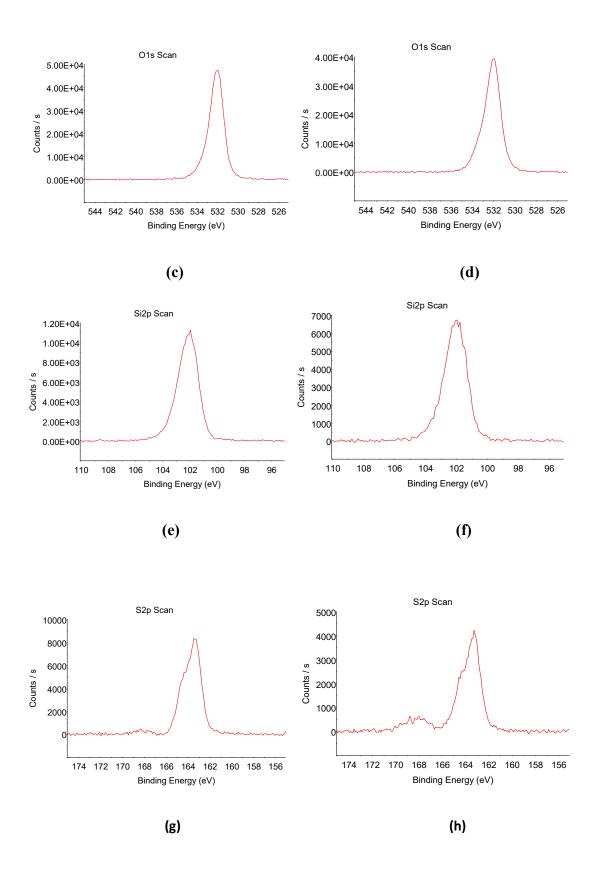
	Carbon (%)	Oxygen (%)	Silicon (%)	Sulfur (%)
Thiol modified glass coverslips	68.10	23.06	4.80	1.06
DNA modified glass coverslips without WSP	68.20	22.69	6.51	2.05

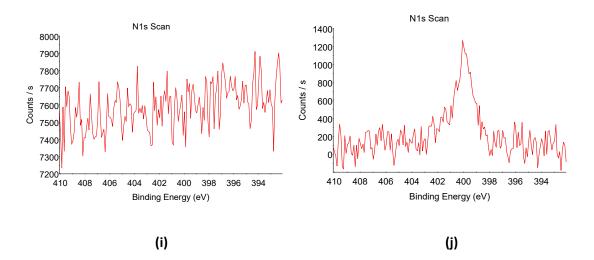




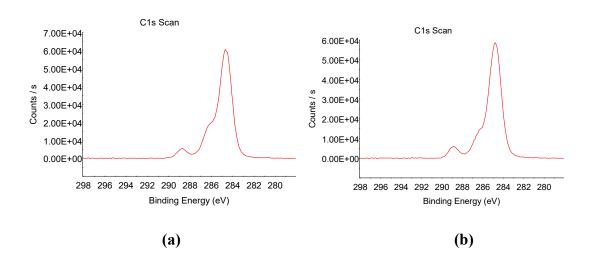
**Figure 18:**XPS graphs of clean glass coverslips and thiol modified coverslips. In above figures, (a),(c),(e) are XPS scans of clean glass coverslips of elements carbon,oxygen and silicon respectively. XPS scan of sulfur not taken for clean glass coverslips;(b),(d), (f),(g) are the XPS scan of thiol modified coverslips of elements carbon,oxygen, silicon and sulfur respectively.

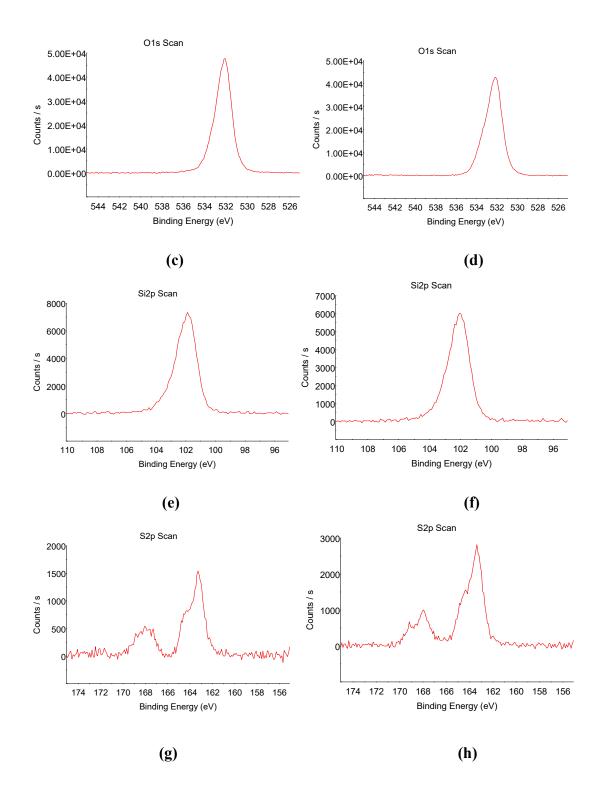






**Figure 19:**XPS graphs of thiol modified and DNA- modified glass coverslips using 0.05% by weight of WSP. In above figures, (a),(c),(e),(g) and(i) are XPS scans of thiol modified glass coverslips of elements carbon,oxygen,silicon, sulfur and nitrogen respectively;(b),(d),(f),(h) are the XPS scan of DNA modified coverslips of elements in the same order as mentioned earlier.





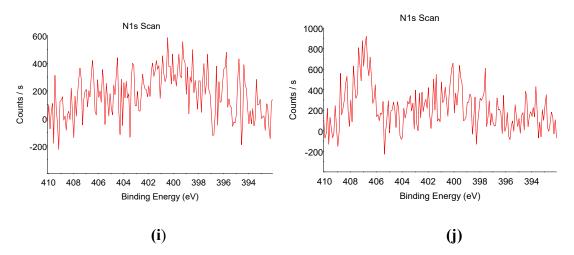


**Figure 20:**XPS graphs of thiol modified and DNA- modified glass coverslips without WSP. In above figures, (a),(c),(e),(g) and(i) are XPS scans of thiol modified glass coverslips of elements carbon,oxygen,silicon, sulfur and nitrogen respectively;(b),(d),(f),(h) are the XPS scan of DNA modified coverslips of elements in the same order as mentioned earlier.

#### References

- 1. Rahman, I.A. and V. Padavettan, Synthesis of silica nanoparticles by sol-gel: size-dependent properties, surface modification, and applications in silica-polymer nanocomposites—a review. Journal of Nanomaterials, 2012. 2012.
- 2. Tan, B. and S.E. Rankin, *Interfacial alignment mechanism of forming spherical silica with radially oriented nanopores*. The Journal of Physical Chemistry B, 2004. **108**(52): p. 20122-20129.
- 3. Hench, L.L. and J.K. West, *The sol-gel process*. Chemical reviews, 1990. **90**(1): p. 33-72.
- 4. Julbe, A., et al., Effect of non-ionic surface active agents on teos-derived sols, gels and materials. Journal of Sol-Gel Science and Technology, 1995. 4(2): p. 89-97.
- 5. Brinker, C.J. and G.W. Scherer, *Sol-gel science: the physics and chemistry of sol-gel processing.* 2013: Academic press.
- 6. Han, Y., et al., Unraveling the growth mechanism of silica particles in the Stöber method: in situ seeded growth model. Langmuir, 2017. **33**(23): p. 5879-5890.
- 7. Righini, G.C. and A. Chiappini, *Glass optical waveguides: a review of fabrication techniques*. Optical Engineering, 2014. **53**(7): p. 071819.
- 8. Davis, M.E. and R.F. Lobo, *Zeolite and molecular sieve synthesis*. Chemistry of Materials, 1992. **4**(4): p. 756-768.
- 9. Beretta, M., Nanostructured mesoporous materials obtained by template synthesis and controlled shape replica. 2009.
- 10. Brinker, C.J., et al., *Evaporation-induced self-assembly: nanostructures made easy.* Advanced materials, 1999. **11**(7): p. 579-585.
- 11. Iler, K.R., *The chemistry of silica*. Solubility, Polymerization, Colloid and Surface Properties and Biochemistry of Silica, 1979.
- 12. Sayari, A., Periodic mesoporous materials: synthesis, characterization and potential applications, in Studies in Surface Science and Catalysis. 1996, Elsevier. p. 1-46.
- 13. Wu, S.-H., C.-Y. Mou, and H.-P. Lin, *Synthesis of mesoporous silica nanoparticles*. Chemical Society Reviews, 2013. **42**(9): p. 3862-3875.
- 14. Suzuki, K., K. Ikari, and H. Imai, Synthesis of silica nanoparticles having a well-ordered mesostructure using a double surfactant system. Journal of the American Chemical Society, 2004. **126**(2): p. 462-463.
- 15. Stöber, W., A. Fink, and E. Bohn, *Controlled growth of monodisperse silica spheres in the micron size range*. Journal of colloid and interface science, 1968. **26**(1): p. 62-69.
- 16. Grün, M., I. Lauer, and K.K. Unger, *The synthesis of micrometer-and submicrometer-size spheres of ordered mesoporous oxide MCM-41*. Advanced Materials, 1997. **9**(3): p. 254-257.
- 17. Yano, K. and Y. Fukushima, *Synthesis of mono-dispersed mesoporous silica spheres with highly ordered hexagonal regularity using conventional alkyltrimethylammonium halide as a surfactant.* Journal of Materials Chemistry, 2004. **14**(10): p. 1579-1584.
- 18. Nakamura, T., et al., Formation mechanism for monodispersed mesoporous silica spheres and its application to the synthesis of core/shell particles. The Journal of Physical Chemistry C, 2007. **111**(3): p. 1093-1100.

- 19. Pauwels, B., et al., *Structure Determination of Spherical MCM-41 Particles*. Advanced Materials, 2001. **13**(17): p. 1317-1320.
- 20. Nooney, R.I., et al., *Synthesis of nanoscale mesoporous silica spheres with controlled particle size*. Chemistry of materials, 2002. **14**(11): p. 4721-4728.
- 21. Van Tendeloo, G., et al., *Structure of nanoscale mesoporous silica spheres?* Journal of Physics: Condensed Matter, 2003. **15**(42): p. S3037.
- 22. Lebedev, O.I., et al., *Structure and microstructure of nanoscale mesoporous silica spheres*. Solid state sciences, 2004. **6**(5): p. 489-498.
- 23. Kresge, C., et al., *Ordered mesoporous molecular sieves synthesized by a liquid-crystal template mechanism.* nature, 1992. **359**(6397): p. 710-712.
- 24. Corma, A., et al., Synthesis of MCM-41 with different pore diameters without addition of auxiliary organics. Chemistry of materials, 1997. **9**(10): p. 2123-2126.
- 25. Prouzet, E. and T.J. Pinnavaia, Assembly of mesoporous molecular sieves containing wormhole motifs by a nonionic surfactant pathway: control of pore size by synthesis temperature. Angewandte Chemie International Edition in English, 1997. **36**(5): p. 516-518.
- 26. Swar, S., V. Máková, and I. Stibor, Effectiveness of Diverse Mesoporous Silica Nanoparticles as Potent Vehicles for the Drug L-DOPA. Materials, 2019. **12**(19): p. 3202.
- 27. Eeman, M. and M. Deleu, From biological membranes to biomimetic model membranes. Base, 2010.
- 28. Brown, D. and E. London, *Structure and origin of ordered lipid domains in biological membranes*. Journal of Membrane Biology, 1998. **164**(2): p. 103-114.
- 29. Yeagle, P.L., *Lipid regulation of cell membrane structure and function*. The FASEB journal, 1989. **3**(7): p. 1833-1842.
- 30. Bloom, M., E. Evans, and O.G. Mouritsen, *Physical properties of the fluid lipid-bilayer component of cell membranes: a perspective*. Quarterly reviews of biophysics, 1991. **24**(3): p. 293-397.
- 31. Smith, B.D., et al., Facilitated transport of carbohydrates, catecholamines, and amino acids through liquid and plasticized organic membranes. Journal of inclusion phenomena and molecular recognition in chemistry, 1998. **32**(2-3): p. 121-131.
- 32. Zhou, S., et al., *Lipid pore-filled silica thin-film membranes for biomimetic recovery of dilute carbohydrates*. Langmuir, 2017. **33**(49): p. 14156-14166.
- 33. Lorin, A., et al., *Les liposomes: description, fabrication et applications.* BASE, 2004.
- 34. Mui, B., L. Chow, and M.J. Hope, *Extrusion technique to generate liposomes of defined size*. Methods in enzymology, 2003. **367**: p. 3.
- 35. MacDonald, R.C., et al., *Small-volume extrusion apparatus for preparation of large, unilamellar vesicles*. Biochimica et Biophysica Acta (BBA)-Biomembranes, 1991. **1061**(2): p. 297-303.
- 36. Akbarzadeh, A., et al., *Liposome: classification, preparation, and applications.* Nanoscale research letters, 2013. **8**(1): p. 102.
- 37. Pinheiro, M., et al., *Liposomes as drug delivery systems for the treatment of TB*. Nanomedicine, 2011. **6**(8): p. 1413-1428.
- 38. Lasic, D.D., *Novel applications of liposomes*. Trends in biotechnology, 1998. **16**(7): p. 307-321.

- 39. Grit, M. and D.J. Crommelin, *Chemical stability of liposomes: implications for their physical stability*. Chemistry and physics of lipids, 1993. **64**(1-3): p. 3-18.
- 40. Roy, B., et al., *Influence of lipid composition, pH, and temperature on physicochemical properties of liposomes with curcumin as model drug.* Journal of oleo science, 2016. **65**(5): p. 399-411.
- 41. Lichtenberg, D. and Y. Barenholz, *Liposomes: preparation, characterization, and preservation.* Methods Biochem. Anal, 1988. **33**: p. 337-462.
- 42. Armengol, X. and J. Estelrich, *Physical stability of different liposome compositions obtained by extrusion method.* Journal of microencapsulation, 1995. **12**(5): p. 525-535.
- 43. Puskás, I. and F. Csempesz, *Influence of cyclodextrins on the physical stability of DPPC-liposomes*. Colloids and surfaces B: biointerfaces, 2007. **58**(2): p. 218-224.
- 44. Zhou, S., Pore-confined Carriers and Biomolecules in Mesoporous Silica for Biomimetic Separation and Targeting. 2017.
- 45. Kokkona, M., et al., Stability of SUV liposomes in the presence of cholate salts and pancreatic lipases: effect of lipid composition. European journal of pharmaceutical sciences, 2000. **9**(3): p. 245-252.
- 46. Boxer, S.G., *Molecular transport and organization in supported lipid membranes*. Current opinion in chemical biology, 2000. **4**(6): p. 704-709.
- 47. Mingeot-Leclercq, M.-P., et al., *Atomic force microscopy of supported lipid bilayers*. Nature protocols, 2008. **3**(10): p. 1654.
- 48. Loose, M. and P. Schwille, *Biomimetic membrane systems to study cellular organization*. Journal of structural biology, 2009. **168**(1): p. 143-151.
- 49. Rossi, C. and J. Chopineau, *Biomimetic tethered lipid membranes designed for membrane-protein interaction studies*. European Biophysics Journal, 2007. **36**(8): p. 955-965.
- 50. Buranda, T., et al., *Biomimetic molecular assemblies on glass and mesoporous silica microbeads for biotechnology*. Langmuir, 2003. **19**(5): p. 1654-1663.
- 51. Ashley, C.E., et al., *Delivery of small interfering RNA by peptide-targeted mesoporous silica nanoparticle-supported lipid bilayers*. ACS nano, 2012. **6**(3): p. 2174-2188.
- 52. Ashley, C.E., et al., *The targeted delivery of multicomponent cargos to cancer cells by nanoporous particle-supported lipid bilayers*. Nature materials, 2011. **10**(5): p. 389-397.
- 53. Schlipf, D.M., et al., Effects of pore size and tethering on the diffusivity of lipids confined in mesoporous silica. Advanced Materials Interfaces, 2017. **4**(9): p. 1601103.
- 54. Nishiyabu, R., et al., *Boronic acid building blocks: tools for sensing and separation*. Chemical Communications, 2011. **47**(4): p. 1106-1123.
- 55. Wang, X., N. Xia, and L. Liu, *Boronic acid-based approach for separation and immobilization of glycoproteins and its application in sensing*. International journal of molecular sciences, 2013. **14**(10): p. 20890-20912.
- 56. Mallia, A.K., et al., *Preparation and use of a boronic acid affinity support for separation and quantitation of glycosylated hemoglobins*. Analytical Letters, Part B: Clinical and Biochemical Analysis, 1981. **14**(8): p. 649-661.
- 57. Xu, Z., et al., Fluorescent boronic acid polymer grafted on silica particles for affinity separation of saccharides. ACS applied materials & interfaces, 2014. **6**(3): p. 1406-1414.

- 58. Meiland, M., et al., Seven-membered ring boronates at trans-diol moieties of carbohydrates. Tetrahedron Letters, 2009. **50**(4): p. 469-472.
- 59. Xie, W., et al., Effect of potassium perfluorooctanesulfonate, perfluorooctanoate and octanesulfonate on the phase transition of dipalmitoylphosphatidylcholine (DPPC) bilayers. Biochimica et Biophysica Acta (BBA)-Biomembranes, 2007. 1768(5): p. 1299-1308.
- 60. Lehmler, H.-J., et al., Mixing of perfluorooctanesulfonic acid (PFOS) potassium salt with dipalmitoyl phosphatidylcholine (DPPC). Colloids and Surfaces B: Biointerfaces, 2006. **51**(1): p. 25-29.
- 61. McElhaney, R.N., *The use of differential scanning calorimetry and differential thermal analysis in studies of model and biological membranes.* Chemistry and physics of lipids, 1982. **30**(2-3): p. 229-259.
- 62. Freire, E., *Differential scanning calorimetry*, in *Protein stability and folding*. 1995, Springer. p. 191-218.
- 63. Biltonen, R.L. and D. Lichtenberg, *The use of differential scanning calorimetry* as a tool to characterize liposome preparations. Chemistry and physics of lipids, 1993. **64**(1-3): p. 129-142.
- 64. netzsch-thermal-analysis. Functional principle of a heat-flux DSC. n.d.
- 65. Janiak, M.J., D.M. Small, and G.G. Shipley, *Temperature and compositional dependence of the structure of hydrated dimyristoyl lecithin*. Journal of Biological Chemistry, 1979. **254**(13): p. 6068-6078.
- 66. McElhaney, R.N.A.H.L.a.R.N., *The Structure of Biological Membranes*. 3rd edition ed. Vol. vol. 2. 2005.: CRC press.
- 67. Pabst, G., et al., Structure and fluctuations of phosphatidylcholines in the vicinity of the main phase transition. Physical Review E, 2004. **70**(2): p. 021908.
- 68. McIntosh, T., Differences in hydrocarbon chain tilt between hydrated phosphatidylethanolamine and phosphatidylcholine bilayers. A molecular packing model. Biophysical journal, 1980. **29**(2): p. 237-245.
- 69. Janiak, M.J., D.M. Small, and G.G. Shipley, *Nature of the thermal pretransition of synthetic phospholipids: dimyristoyl-and dipalmitoyllecithin.* Biochemistry, 1976. **15**(21): p. 4575-4580.
- 70. Heimburg, T., A model for the lipid pretransition: coupling of ripple formation with the chain-melting transition. Biophysical journal, 2000. **78**(3): p. 1154-1165.
- 71. Barba, A.A., et al., *Polymeric and lipid-based systems for controlled drug release: an engineering point of view*, in *Nanomaterials for Drug Delivery and Therapy*. 2019, Elsevier. p. 267-304.
- 72. Kulkarni, V.S., *Handbook of non-invasive drug delivery systems: science and technology.* 2009: Elsevier.
- 73. Selvamani, V., Stability Studies on Nanomaterials Used in Drugs, in Characterization and Biology of Nanomaterials for Drug Delivery. 2019, Elsevier. p. 425-444.
- 74. Caputo, F. Measuring Zeta Potential. 2015.
- 75. Abbott, S. *PRACTICAL SOLUBILITY DISPERSIONS*. Available from: <a href="https://www.stevenabbott.co.uk/practical-solubility/zeta.php">https://www.stevenabbott.co.uk/practical-solubility/zeta.php</a>.
- 76. Bhattacharjee, S., *DLS and zeta potential—what they are and what they are not?* Journal of Controlled Release, 2016. **235**: p. 337-351.

- 77. Joseph, E. and G. Singhvi, *Multifunctional nanocrystals for cancer therapy: A potential nanocarrier*, in *Nanomaterials for Drug Delivery and Therapy*. 2019, Elsevier. p. 91-116.
- 78. Krstić, M., et al., Self-nanoemulsifying drug delivery systems (SNEDDS) and self-microemulsifying drug delivery systems (SMEDDS) as lipid nanocarriers for improving dissolution rate and bioavailability of poorly soluble drugs, in Lipid nanocarriers for drug targeting. 2018, Elsevier. p. 473-508.
- 79. Gumustas, M., et al., Effect of polymer-based nanoparticles on the assay of antimicrobial drug delivery systems, in Multifunctional systems for combined delivery, biosensing and diagnostics. 2017, Elsevier. p. 67-108.
- 80. Gupta, V. and P. Trivedi, In vitro and in vivo characterization of pharmaceutical topical nanocarriers containing anticancer drugs for skin cancer treatment, in Lipid Nanocarriers for Drug Targeting. 2018, Elsevier. p. 563-627.
- 81. Pan, H., et al., *Postformulation peptide drug loading of nanostructures*, in *Methods in enzymology*. 2012, Elsevier. p. 17-39.
- 82. Singh, G. and L. Song, Experimental correlations of pH and ionic strength effects on the colloidal fouling potential of silica nanoparticles in crossflow ultrafiltration. Journal of membrane science, 2007. **303**(1-2): p. 112-118.
- 83. Júnior, J.A.A. and J.B. Baldo, *The behavior of zeta potential of silica suspensions*. New Journal of Glass and Ceramics, 2014. **4**(02): p. 29.
- 84. Metin, C.O., et al., *Stability of aqueous silica nanoparticle dispersions*. Journal of Nanoparticle Research, 2011. **13**(2): p. 839-850.
- 85. Savarala, S., et al., Formation and colloidal stability of DMPC supported lipid bilayers on SiO2 nanobeads. Langmuir, 2010. **26**(14): p. 12081-12088.
- 86. Moura, S.P. and A.M. Carmona-Ribeiro, *Biomimetic particles: optimization of phospholipid bilayer coverage on silica and colloid stabilization*. Langmuir, 2005. **21**(22): p. 10160-10164.
- 87. Ribeiro, R.T., V.H. Braga, and A.M. Carmona-Ribeiro, *Biomimetic cationic nanoparticles based on silica: Optimizing bilayer deposition from lipid films*. Biomimetics, 2017. **2**(4): p. 20.
- 88. Moura, S.P. and A.M. Carmona-Ribeiro, *Cationic bilayer fragments on silica* at low ionic strength: competitive adsorption and colloid stability. Langmuir, 2003. **19**(17): p. 6664-6667.
- 89. Rand, R., *Interacting phospholipid bilayers: measured forces and induced structural changes*. Annual review of biophysics and bioengineering, 1981. **10**(1): p. 277-314.
- 90. Argyo, C., et al., Multifunctional mesoporous silica nanoparticles as a universal platform for drug delivery. Chemistry of Materials, 2014. **26**(1): p. 435-451.
- 91. Lin, Y.-S., et al., *Well-ordered mesoporous silica nanoparticles as cell markers*. Chemistry of Materials, 2005. **17**(18): p. 4570-4573.
- 92. Singh, N., et al., *Bioresponsive mesoporous silica nanoparticles for triggered drug release*. Journal of the American Chemical Society, 2011. **133**(49): p. 19582-19585.
- 93. Narayan, R., et al., *Mesoporous silica nanoparticles: A comprehensive review on synthesis and recent advances.* Pharmaceutics, 2018. **10**(3): p. 118.
- 94. Li, Z., et al., Mesoporous silica nanoparticles in biomedical applications. Chemical Society Reviews, 2012. **41**(7): p. 2590-2605.

- 95. Wang, Y., et al., *Mesoporous silica nanoparticles in drug delivery and biomedical applications*. Nanomedicine: Nanotechnology, Biology and Medicine, 2015. **11**(2): p. 313-327.
- 96. Vivero-Escoto, J.L., et al., *Mesoporous silica nanoparticles for intracellular controlled drug delivery*. Small, 2010. **6**(18): p. 1952-1967.
- 97. Slowing, I.I., et al., *Mesoporous silica nanoparticles for drug delivery and biosensing applications*. Advanced Functional Materials, 2007. **17**(8): p. 1225-1236.
- 98. Yang, Y. and J. Li, Lipid, protein and poly (NIPAM) coated mesoporous silica nanoparticles for biomedical applications. Advances in colloid and interface science, 2014. **207**: p. 155-163.
- 99. Brian, A.A. and H.M. McConnell, *Allogeneic stimulation of cytotoxic T cells by supported planar membranes*. Proceedings of the National Academy of Sciences, 1984. **81**(19): p. 6159-6163.
- 100. Girard-Egrot, A.P. and L.J. Blum, *Langmuir-Blodgett technique for synthesis of biomimetic lipid membranes*, in *Nanobiotechnology of biomimetic membranes*. 2007, Springer. p. 23-74.
- 101. Yang, Y., et al., *Lipid coated mesoporous silica nanoparticles as photosensitive drug carriers*. Physical Chemistry Chemical Physics, 2010. **12**(17): p. 4418-4422.
- 102. Cauda, V., et al., Colchicine-loaded lipid bilayer-coated 50 nm mesoporous nanoparticles efficiently induce microtubule depolymerization upon cell uptake. Nano letters, 2010. **10**(7): p. 2484-2492.
- 103. van Schooneveld, M.M., et al., *A fluorescent, paramagnetic and PEGylated gold/silica nanoparticle for MRI, CT and fluorescence imaging.* Contrast media & molecular imaging, 2010. **5**(4): p. 231-236.
- 104. Valange, S., et al., Nanoparticles of Fe2O3 inserted in SBA-15 silica at micropore mouth level: An experimental evidence of the confinement effect. Journal of Molecular Catalysis A: Chemical, 2009. **305**(1-2): p. 24-33.
- 105. Chiche, B., et al., *Butene oligomerization over mesoporous MTS-type aluminosilicates*. Journal of Molecular Catalysis A: Chemical, 1998. **134**(1-3): p. 145-157.
- 106. Iwamoto, M., et al., Remarkable effect of pore size on the catalytic activity of mesoporous silica for the acetalization of cyclohexanone with methanol. Journal of the American Chemical Society, 2003. **125**(43): p. 13032-13033.
- 107. Ren, Y., Z. Ma, and P.G. Bruce, *Ordered mesoporous metal oxides: synthesis and applications*. Chemical Society Reviews, 2012. **41**(14): p. 4909-4927.
- 108. H. Wang, Q.L., F. Gao, Q. Shi, Y. Yan, F. Zhang, S. Xie, B. Tu, D. Zhao, , Adv. Funct.Mater.,

#### (2005) **15**: p. 1377.

- 109. Falahati, M., et al., *The effect of functionalization of mesoporous silica nanoparticles on the interaction and stability of confined enzyme.* International journal of biological macromolecules, 2012. **50**(4): p. 1048-1054.
- 110. Buntkowsky, G., et al., *Structural and dynamical properties of guest molecules confined in mesoporous silica materials revealed by NMR*. Physical Chemistry Chemical Physics, 2007. **9**(35): p. 4843-4853.
- 111. Liu, J., et al., *Heat-triggered drug release systems based on mesoporous silica nanoparticles filled with a maghemite core and phase-change molecules as gatekeepers.* Journal of Materials Chemistry B, 2014. **2**(1): p. 59-70.

- 112. Jia, L., et al., Successfully tailoring the pore size of mesoporous silica nanoparticles: exploitation of delivery systems for poorly water-soluble drugs. International journal of pharmaceutics, 2012. 439(1-2): p. 81-91.
- 113. Li, C., et al., Compression of ionic liquid when confined in porous silica nanoparticles. RSC advances, 2013. **3**(25): p. 9618-9621.
- 114. Zhang, Y., et al., *Inclusion of telmisartan in mesocellular foam nanoparticles:* drug loading and release property. European journal of pharmaceutics and biopharmaceutics, 2010. **76**(1): p. 17-23.
- 115. Zhang, Y., et al., *Inclusion of the poorly water-soluble drug simvastatin in mesocellular foam nanoparticles: drug loading and release properties.* International journal of pharmaceutics, 2011. **410**(1-2): p. 118-124.
- 116. Thomas, M., et al., *Inclusion of poorly soluble drugs in highly ordered mesoporous silica nanoparticles*. international Journal of Pharmaceutics, 2010. **387**(1-2): p. 272-277.
- 117. Ozawa, R., et al., Rotational isomerism and structure of the 1-butyl-3-methylimidazolium cation in the ionic liquid state. Chemistry Letters, 2003. **32**(10): p. 948-949.
- 118. Elaiwi, A., et al., *Hydrogen bonding in imidazolium salts and its implications for ambient-temperature halogenoaluminate (III) ionic liquids.* Journal of the Chemical Society, Dalton Transactions, 1995(21): p. 3467-3472.
- 119. Li, C., et al., Pt2Cl82-Dimer Formation of [Bmim] 2PtCl4 Ionic Liquid When Confined in Silica Nanopores. The Journal of Physical Chemistry C, 2014. 118(6): p. 3140-3144.
- 120. Singh, M.P., R.K. Singh, and S. Chandra, *Properties of ionic liquid confined in porous silica matrix*. ChemPhysChem, 2010. **11**(9): p. 2036-2043.
- 121. Ueno, K., et al., *Resonance shear measurement of nanoconfined ionic liquids*. Physical Chemistry Chemical Physics, 2010. **12**(16): p. 4066-4071.
- 122. Wang, Y., et al., *The influence of silica nanoparticles on ionic liquid behavior:* a clear difference between adsorption and confinement. International journal of molecular sciences, 2013. **14**(10): p. 21045-21052.
- Duggan, P.J., Fructose-permeable liquid membranes containing boronic acid carriers. Australian journal of chemistry, 2004. 57(4): p. 291-299.
- 124. Gardiner, S.J., et al., Selective fructose transport through supported liquid membranes containing diboronic acid or conjugated monoboronic acid-quaternary ammonium carriers. Tetrahedron, 1999. **55**(10): p. 2857-2864.
- 125. Duggan, P.J., et al., *Enhanced fructose, glucose and lactose transport promoted by a lipophilic 2-(aminomethyl)-phenylboronic acid.* Tetrahedron, 2008. **64**(30-31): p. 7122-7126.
- 126. Walsh, A.J. and H.G. Monbouquette, Extraction of Cd2+ and Pb2+ from dilute aqueous solution using metal-sorbing vesicles in a hollow-fiber cartridge. Journal of membrane science, 1993. **84**(1-2): p. 107-121.
- 127. Powers, J.D., P.K. Kilpatrick, and R.G. Carbonell, *Protein purification by affinity binding to unilamellar vesicles*. Biotechnology and bioengineering, 1989. **33**(2): p. 173-182.
- 128. Smith, B.D., Sugar separation using liquid membranes and boronic acid carriers. 1996, ACS Publications.
- 129. Inoue, T., K. Miyakawa, and R. Shimozawa, *Interaction of surfactants with vesicle membrane of dipalmitoylphosphatidylcholine. Effect on gel-to-liquid-crystalline phase transition of lipid bilayer*. Chemistry and physics of lipids, 1986. **42**(4): p. 261-270.

- 130. Koynova, R. and M. Caffrey, *Phases and phase transitions of the phosphatidylcholines*. Biochimica et Biophysica Acta (BBA)-Reviews on Biomembranes, 1998. **1376**(1): p. 91-145.
- 131. Mesa, M., et al., Preparation of micron-sized spherical particles of mesoporous silica from a triblock copolymer surfactant, usable as a stationary phase for liquid chromatography. Solid State Sciences, 2003. 5(9): p. 1303-1308.
- 132. Thommes, M., et al., *Physisorption of gases, with special reference to the evaluation of surface area and pore size distribution (IUPAC Technical Report)*. Pure and Applied Chemistry, 2015. **87**(9-10): p. 1051-1069.
- 133. Barron, P.M.V.R.A.R. *BET Surface Area Analysis of Nanoparticles*. Jan 10,2020; Available from: <a href="https://chem.libretexts.org/Bookshelves/Analytical\_Chemistry/Book%3A\_Physical\_Methods\_in\_Chemistry\_and\_Nano\_Science\_(Barron)/02%3A\_Physical\_and\_Thermal\_Analysis/2.03%3A\_BET\_Surface\_Area\_Analysis\_of\_Nanopar\_ticles.</a>
- 134. Ganesh, M., et al., Development of duloxetine hydrochloride loaded mesoporous silica nanoparticles: characterizations and in vitro evaluation. AAPS PharmSciTech, 2015. **16**(4): p. 944-951.
- 135. Phanasgaonkar, A. and V. Raja, *Influence of curing temperature, silica nanoparticles-and cerium on surface morphology and corrosion behaviour of hybrid silane coatings on mild steel.* Surface and Coatings Technology, 2009. **203**(16): p. 2260-2271.
- 136. Miyoshi, T., et al., A detailed analysis of partial molecular volumes in DPPC/cholesterol binary bilayers. Biochimica et Biophysica Acta (BBA)-Biomembranes, 2014. **1838**(12): p. 3069-3077.
- 137. Schlipf, D.M., Biomolecule localization and surface engineering within size tunable nanoporous silica particles. 2015.
- 138. Lundbæk, J.A., et al., *Lipid bilayer regulation of membrane protein function:* gramicidin channels as molecular force probes. Journal of The Royal Society Interface, 2010. **7**(44): p. 373-395.
- 139. Demetzos, C., Differential scanning calorimetry (DSC): a tool to study the thermal behavior of lipid bilayers and liposomal stability. Journal of liposome research, 2008. **18**(3): p. 159-173.
- 140. Müter, D., et al., Surfactant self-assembly in cylindrical silica nanopores. The Journal of Physical Chemistry Letters, 2010. **1**(9): p. 1442-1446.
- 141. Ojogun, V., et al., *Partitioning of homologous nicotinic acid ester prodrugs* (nicotinates) into dipalmitoylphosphatidylcholine (DPPC) membrane bilayers. Colloids and Surfaces B: Biointerfaces, 2010. **78**(1): p. 75-84.
- 142. Avila, C.M. and F. Martinez, *Thermodynamics of partitioning of benzocaine in some organic solvent/buffer and liposome systems*. Chemical and pharmaceutical bulletin, 2003. **51**(3): p. 237-240.
- 143. Nagle, J.F., *Theory of the main lipid bilayer phase transition*. Annual Review of Physical Chemistry, 1980. **31**(1): p. 157-196.
- 144. Prenner, E.J., et al., Differential scanning calorimetric study of the effect of the antimicrobial peptide gramicidin S on the thermotropic phase behavior of phosphatidylcholine, phosphatidylethanolamine and phosphatidylglycerol lipid bilayer membranes. Biochimica et Biophysica Acta (BBA)-Biomembranes, 1999. 1417(2): p. 211-223.

- 145. Ohline, S.M., et al., Differential scanning calorimetric study of bilayer membrane phase transitions. A biophysical chemistry experiment. Journal of Chemical Education, 2001. **78**(9): p. 1251.
- 146. Ropel, L., et al., Octanol-water partition coefficients of imidazolium-based ionic liquids. Green Chemistry, 2005. 7(2): p. 83-90.
- 147. Xiang, T.-X. and B.D. Anderson, *Liposomal drug transport: a molecular perspective from molecular dynamics simulations in lipid bilayers*. Advanced drug delivery reviews, 2006. **58**(12-13): p. 1357-1378.
- 148. Grossfield, A. and T.B. Woolf, *Interaction of tryptophan analogs with POPC lipid bilayers investigated by molecular dynamics calculations*. Langmuir, 2002. **18**(1): p. 198-210.
- 149. Neunert, G., et al., Partition of tocopheryl glucopyranoside into liposome membranes studied by fluorescence methods. Biophysical chemistry, 2010. **146**(2-3): p. 92-97.
- 150. Guzmán, E., et al., Effect of hydrophilic and hydrophobic nanoparticles on the surface pressure response of DPPC monolayers. The Journal of Physical Chemistry C, 2011. 115(44): p. 21715-21722.
- 151. Guzmán, E., et al., *Mixed DPPC-cholesterol Langmuir monolayers in presence of hydrophilic silica nanoparticles*. Colloids and Surfaces B: Biointerfaces, 2013. **105**: p. 284-293.
- 152. Guzmán, E., et al., *Influence of silica nanoparticles on phase behavior and structural properties of DPPC—Palmitic acid Langmuir monolayers*. Colloids and Surfaces A: Physicochemical and Engineering Aspects, 2012. **413**: p. 280-287.
- 153. Guzmán, E., et al., *DPPC–DOPC Langmuir monolayers modified by hydrophilic silica nanoparticles: Phase behaviour, structure and rheology.* Colloids and Surfaces A: Physicochemical and Engineering Aspects, 2012. **413**: p. 174-183.
- 154. Chunbo, Y., et al., A NMR study of the interaction of silica with dipalmitoylphosphatidylcholine liposomes. Journal of colloid and interface science, 1995. 172(2): p. 536-538.
- 155. Pan, L., et al., Nuclear-targeted drug delivery of TAT peptide-conjugated monodisperse mesoporous silica nanoparticles. Journal of the American Chemical Society, 2012. **134**(13): p. 5722-5725.
- 156. Song, N. and Y.-W. Yang, *Molecular and supramolecular switches on mesoporous silica nanoparticles*. Chemical Society Reviews, 2015. **44**(11): p. 3474-3504.
- 157. Yamamoto, E. and K. Kuroda, *Colloidal mesoporous silica nanoparticles*. Bulletin of the Chemical Society of Japan, 2016. **89**(5): p. 501-539.
- 158. Zhang, Q., R. Huang, and L.-H. Guo, *One-step and high-density protein immobilization on epoxysilane-modified silica nanoparticles*. Chinese Science Bulletin, 2009. **54**(15): p. 2620-2626.
- 159. Mohapatra, S., et al., Characterization and Biology of Nanomaterials for Drug Delivery: Nanoscience and Nanotechnology in Drug Delivery. 2018: Elsevier.
- 160. Nooney, R.I., et al., *Investigating the colloidal stability of fluorescent silica nanoparticles under isotonic conditions for biomedical applications*. Journal of colloid and interface science, 2015. **456**: p. 50-58.
- 161. Selvaggi, R., et al., Silica nanoparticles assisted photodegradation of acridine orange in aqueous suspensions. Applied Catalysis B: Environmental, 2015. **168**: p. 363-369.

- 162. Sardan, M., et al., *Noncovalent functionalization of mesoporous silica nanoparticles with amphiphilic peptides*. Journal of Materials Chemistry B, 2014. **2**(15): p. 2168-2174.
- 163. Meissner, J., et al., Characterization of protein adsorption onto silica nanoparticles: influence of pH and ionic strength. Colloid and polymer science, 2015. **293**(11): p. 3381-3391.
- 164. Gun'ko, V., et al., Effects of dissolved metal chlorides on the behavior of silica nanoparticles in aqueous media. Open Chemistry, 2014. **12**(4): p. 480-491.
- 165. Shen, S.-C., et al., Sonochemical synthesis of (3-aminopropyl) triethoxysilane-modified monodispersed silica nanoparticles for protein immobilization. Materials Research Bulletin, 2011. **46**(10): p. 1665-1669.
- 166. Gong, Z.-S., L.-P. Duan, and A.-N. Tang, *Amino-functionalized silica* nanoparticles for improved enantiomeric separation in capillary electrophoresis using carboxymethyl-β-cyclodextrin (CM-β-CD) as a chiral selector. Microchimica Acta, 2015. **182**(7-8): p. 1297-1304.
- 167. Jesionowski, T., Influence of aminosilane surface modification and dyes adsorption on zeta potential of spherical silica particles formed in emulsion system. Colloids and Surfaces A: Physicochemical and Engineering Aspects, 2003. 222(1-3): p. 87-94.
- 168. Arnaut, L. and H. Burrows, *Chemical kinetics: from molecular structure to chemical reactivity*. 2006: Elsevier.
- 169. Gelardi, G. and R. Flatt, Working mechanisms of water reducers and superplasticizers, in Science and Technology of Concrete Admixtures. 2016, Elsevier. p. 257-278.
- 170. Wang, D., et al., *Bridging interactions and selective nanoparticle aggregation mediated by monovalent cations*. ACS nano, 2011. **5**(1): p. 530-536.
- 171. Sofla, S.J.D., L.A. James, and Y. Zhang, *Insight into the stability of hydrophilic silica nanoparticles in seawater for Enhanced oil recovery implications*. Fuel, 2018. **216**: p. 559-571.
- 172. Morrison, I.D., Criterion for electrostatic stability of dispersions at low ionic strength. Langmuir, 1991. 7(9): p. 1920-1922.
- 173. Nobbmann, B.U. *DEBYE SCREENING HOW IT AFFECTS ZETA POTENTIAL*. 2018; Available from: <a href="https://www.materials-talks.com/blog/2018/10/03/debye-screening-how-it-affects-zeta-potential/">https://www.materials-talks.com/blog/2018/10/03/debye-screening-how-it-affects-zeta-potential/</a>.
- 174. Kim, K.-M., et al., Surface treatment of silica nanoparticles for stable and charge-controlled colloidal silica. International journal of nanomedicine, 2014. **9**(Suppl 2): p. 29.
- 175. Castellana, E.T. and P.S. Cremer, *Solid supported lipid bilayers: From biophysical studies to sensor design*. Surface Science Reports, 2006. **61**(10): p. 429-444.
- 176. Richter, R.P., R. Bérat, and A.R. Brisson, *Formation of solid-supported lipid bilayers: an integrated view.* Langmuir, 2006. **22**(8): p. 3497-3505.
- 177. Yamada, H., et al., A multifunctional role of trialkylbenzenes for the preparation of aqueous colloidal mesostructured/mesoporous silica nanoparticles with controlled pore size, particle diameter, and morphology. Nanoscale, 2015. 7(46): p. 19557-19567.
- 178. Yu, M., et al., *Hyaluronic acid modified mesoporous silica nanoparticles for targeted drug delivery to CD44-overexpressing cancer cells.* Nanoscale, 2013. **5**(1): p. 178-183.

- 179. Brown, M.A., A. Goel, and Z. Abbas, *Effect of electrolyte concentration on the stern layer thickness at a charged interface*. Angewandte Chemie International Edition, 2016. **55**(11): p. 3790-3794.
- 180. Leekumjorn, S. and A.K. Sum, *Molecular simulation study of structural and dynamic properties of mixed DPPC/DPPE bilayers*. Biophysical journal, 2006. **90**(11): p. 3951-3965.
- 181. Roggers, R.A., V.S.-Y. Lin, and B.G. Trewyn, *Chemically reducible lipid bilayer coated mesoporous silica nanoparticles demonstrating controlled release and HeLa and normal mouse liver cell biocompatibility and cellular internalization*. Molecular pharmaceutics, 2012. **9**(9): p. 2770-2777.
- 182. Anderson, T.H., et al., Formation of supported bilayers on silica substrates. Langmuir, 2009. **25**(12): p. 6997-7005.
- 183. Park, Y., et al., Colloidal dispersion stability of unilamellar DPPC vesicles in aqueous electrolyte solutions and comparisons to predictions of the DLVO theory. Journal of colloid and interface science, 2010. **342**(2): p. 300-310.
- 184. Richter, R., A. Mukhopadhyay, and A. Brisson, *Pathways of lipid vesicle deposition on solid surfaces: a combined QCM-D and AFM study.* Biophysical journal, 2003. **85**(5): p. 3035-3047.
- 185. Reimhult, E., F. Höök, and B. Kasemo, *Vesicle adsorption on SiO 2 and TiO 2: dependence on vesicle size*. The Journal of chemical physics, 2002. **117**(16): p. 7401-7404.
- 186. Mornet, S., et al., *The formation of supported lipid bilayers on silica nanoparticles revealed by cryoelectron microscopy.* Nano letters, 2005. **5**(2): p. 281-285.
- 187. Yang, Q., et al., pH-responsive carrier system based on carboxylic acid modified mesoporous silica and polyelectrolyte for drug delivery. Chemistry of Materials, 2005. 17(24): p. 5999-6003.
- 188. Popat, A., et al., *A pH-responsive drug delivery system based on chitosan coated mesoporous silica nanoparticles*. Journal of Materials Chemistry, 2012. **22**(22): p. 11173-11178.
- 189. Feng, W., et al., *Polyelectrolyte multilayer functionalized mesoporous silica nanoparticles for pH-responsive drug delivery: layer thickness-dependent release profiles and biocompatibility.* Journal of Materials Chemistry B, 2013. **1**(43): p. 5886-5898.
- 190. Yuan, L., et al., *Preparation of pH-responsive mesoporous silica nanoparticles and their application in controlled drug delivery*. The Journal of Physical Chemistry C, 2011. **115**(20): p. 9926-9932.
- 191. Xu, H., et al., A facile route for rapid synthesis of hollow mesoporous silica nanoparticles as pH-responsive delivery carrier. Journal of colloid and interface science, 2015. **451**: p. 101-107.
- 192. Gao, Q., et al., *pH-responsive drug release from polymer-coated mesoporous silica spheres*. The Journal of Physical Chemistry C, 2009. **113**(29): p. 12753-12758.
- 193. Hülsmann, S., et al., *Limitations of Sulforhodamine 101 for brain imaging*. Frontiers in cellular neuroscience, 2017. **11**: p. 44.
- 194. Chevalier, A., et al., Azobenzene-caged sulforhodamine dyes: a novel class of 'turn-on'reactive probes for hypoxic tumor cell imaging. Methods and applications in fluorescence, 2015. **3**(4): p. 044004.

- 195. Chevalier, A., P.-Y. Renard, and A. Romieu, *Azo-sulforhodamine dyes: a novel class of broad spectrum dark quenchers*. Organic letters, 2014. **16**(15): p. 3946-3949.
- 196. Kardys, A.Y., D.J. Bharali, and S.A. Mousa, *Amino-functionalized silica* nanoparticles: In vitro evaluation for targeted delivery and therapy of pancreatic cancer. Journal of nanotechnology, 2013. **2013**.
- 197. Hao, N., et al., One-step synthesis of amine-functionalized hollow mesoporous silica nanoparticles as efficient antibacterial and anticancer materials. ACS applied materials & interfaces, 2015. 7(2): p. 1040-1045.
- 198. Hartono, S.B., et al., Amine functionalized cubic mesoporous silica nanoparticles as an oral delivery system for curcumin bioavailability enhancement. Nanotechnology, 2016. **27**(50): p. 505605.
- 199. Mahmoodi, N.M., S. Khorramfar, and F. Najafi, *Amine-functionalized silica nanoparticle: Preparation, characterization and anionic dye removal ability.* Desalination, 2011. **279**(1-3): p. 61-68.
- 200. Liu, S., et al., *The influence of the alcohol concentration on the structural ordering of mesoporous silica: cosurfactant versus cosolvent.* The Journal of Physical Chemistry B, 2003. **107**(38): p. 10405-10411.
- 201. Ezzeddine, Z., et al., Divalent heavy metals adsorption onto different types of EDTA-modified mesoporous materials: Effectiveness and complexation rate. Microporous and Mesoporous Materials, 2015. 212: p. 125-136.
- 202. Na, H.K., et al., Efficient functional delivery of siRNA using mesoporous silica nanoparticles with ultralarge pores. Small, 2012. **8**(11): p. 1752-1761.
- 203. Tjong, V., et al., "Smart" DNA interfaces. Chemical Society Reviews, 2014. **43**(5): p. 1612-1626.
- 204. Hu, R., et al., *Nucleic acid-functionalized nanomaterials for bioimaging applications*. Journal of Materials Chemistry, 2011. **21**(41): p. 16323-16334.
- 205. Tan, S.J., et al., Engineering nanocarriers for siRNA delivery. Small, 2011. **7**(7): p. 841-856.
- 206. Roh, Y.H., et al., *Engineering DNA-based functional materials*. Chemical Society Reviews, 2011. **40**(12): p. 5730-5744.
- 207. Escorihuela, J., et al., *Direct covalent attachment of DNA microarrays by rapid thiol–Ene "click" chemistry.* Bioconjugate chemistry, 2014. **25**(3): p. 618-627.
- 208. Smith, E.A., et al., Formation, spectroscopic characterization, and application of sulfhydryl-terminated alkanethiol monolayers for the chemical attachment of DNA onto gold surfaces. Langmuir, 2001. 17(8): p. 2502-2507.
- 209. Lucarelli, F., et al., *Carbon and gold electrodes as electrochemical transducers* for DNA hybridisation sensors. Biosensors and Bioelectronics, 2004. **19**(6): p. 515-530.
- 210. Tam, P.D., et al., *DNA sensor development based on multi-wall carbon nanotubes for label-free influenza virus (type A) detection.* Journal of Immunological Methods, 2009. **350**(1-2): p. 118-124.
- 211. Knickerbocker, T., et al., *DNA-modified diamond surfaces*. Langmuir, 2003. **19**(6): p. 1938-1942.
- 212. Walsh, M.K., X. Wang, and B.C. Weimer, *Optimizing the immobilization of single-stranded DNA onto glass beads*. Journal of Biochemical and Biophysical Methods, 2001. **47**(3): p. 221-231.
- 213. Steinberg, G., et al., *Strategies for covalent attachment of DNA to beads*. Biopolymers: Original Research on Biomolecules, 2004. **73**(5): p. 597-605.

- 214. Pirri, G., et al., Characterization of a polymeric adsorbed coating for DNA microarray glass slides. Analytical chemistry, 2004. **76**(5): p. 1352-1358.
- 215. Situma, C., et al., Fabrication of DNA microarrays onto poly (methyl methacrylate) with ultraviolet patterning and microfluidics for the detection of low-abundant point mutations. Analytical biochemistry, 2005. **340**(1): p. 123-135.
- 216. Kimura, N., One-step immobilization of poly (dT)-modified DNA onto non-modified plastic substrates by UV irradiation for microarrays. Biochemical and biophysical research communications, 2006. **347**(2): p. 477-484.
- 217. Gudnason, H., et al., An inexpensive and simple method for thermally stable immobilization of DNA on an unmodified glass surface: UV linking of poly (T) 10-poly (C) 10-tagged DNA probes. BioTechniques, 2008. **45**(3): p. 261-271.
- 218. Lin, Z., et al., DNA attachment and hybridization at the silicon (100) surface. Langmuir, 2002. **18**(3): p. 788-796.
- 219. Strother, T., R.J. Hamers, and L.M. Smith, Covalent attachment of oligodeoxyribonucleotides to amine-modified Si (001) surfaces. Nucleic acids research, 2000. **28**(18): p. 3535-3541.
- 220. Yin, H., et al., Submicron patterning of DNA oligonucleotides on silicon. Nucleic acids research, 2004. **32**(14): p. e118-e118.
- 221. Escorihuela, J., et al., *DNA microarrays on silicon surfaces through thiol-ene chemistry*. Chemical Communications, 2012. **48**(15): p. 2116-2118.
- 222. Pellegrino, T., et al., *Gel electrophoresis of gold-DNA nanoconjugates*. BioMed Research International, 2007. **2007**.
- 223. Mather, R., Surface modification of textiles by plasma treatments, in Surface modification of textiles. 2009, Elsevier. p. 296-317.
- 224. Mattox, D.M., *Handbook of physical vapor deposition (PVD) processing*. 2010: William Andrew.
- 225. Han, Y., A. Offenhäusser, and S. Ingebrandt, *Detection of DNA hybridization* by a field-effect transistor with covalently attached catcher molecules. Surface and Interface Analysis: An International Journal devoted to the development and application of techniques for the analysis of surfaces, interfaces and thin films, 2006. **38**(4): p. 176-181.
- 226. Shircliff, R.A., et al., Angle-resolved XPS analysis and characterization of monolayer and multilayer silane films for DNA coupling to silica. Langmuir, 2013. **29**(12): p. 4057-4067.
- 227. Li, A., et al., *Electrochemical impedance detection of DNA hybridization based on dendrimer modified electrode.* Biosensors and Bioelectronics, 2007. **22**(8): p. 1716-1722.
- 228. Lee, C.-Y., et al., Surface coverage and structure of mixed DNA/alkylthiol monolayers on gold: characterization by XPS, NEXAFS, and fluorescence intensity measurements. Analytical chemistry, 2006. **78**(10): p. 3316-3325.
- 229. Bertin, A. and H. Schlaad, *Mild and versatile (bio-) functionalization of glass surfaces via thiol— ene photochemistry*. Chemistry of Materials, 2009. **21**(24): p. 5698-5700.

### **VITA**

## Aniruddha Atul Shirodkar

Place of Birth: Mumbai, India

## **EDUCATIONAL INSTITUTIONS AND DEGREES**

- 1. University of Kentucky (UKY), Lexington, KY, USA M.S in Chemical Engineering (expected May 2020)
- 2. Institute of Chemical Technology, Mumbai, India B.Sc., Chemical Engineering (May 2017)

## PROFESSIONAL POSITIONS HELD

- 1. Research Assistant, University of Kentucky, United States August 2017 - Present
- 2. Teaching Assistant, University of Kentucky, United States August 2017 - May 2018